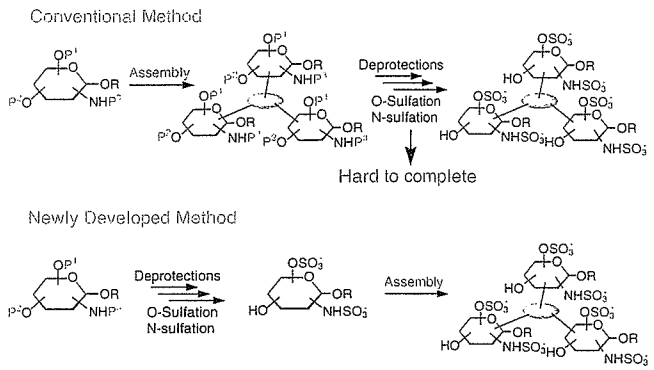

図6　集合化オリゴ糖鎖の調製法

いくつかの方法を検討した結果、還元アミノ化法が硫酸基に影響を与えない最適の方法であることを見出した[13,14]。そのために、最小二糖構造の還元末端側にグルコースを導入した三糖体をまず合成した。また、還元アミノ化反応を詳細に検討したところ、反応液のpHを3～4に保つことが重要であることもわかり、このpH領域で反応が起こるアミノ基として芳香族アミンを有するリンカー化合物を設計した（図7参照）。芳香族アミノ基は疎水性があるため、疎水性相互作用に基づく非特異吸着があることが懸念されるが、グルコースを末端に持つ化合物の場合、反応後グルコース部位が親水性のリンカーとしても働くので、非特異吸着を最少にする効果も期待した。

この方法で、調製した化合物の一例を図8に示す。精製がやや困難であったことから、単離収率は60%程度にとどまっているが、硫酸基の脱離もなく、1ステップで硫酸化二糖を集合化した化合物を調製できた。この化合物の同定・確認には、ちょうど市場にでてきた陰イオンを高分解能、かつ高感度で測定できるESI-TOF/MSが役に立った。

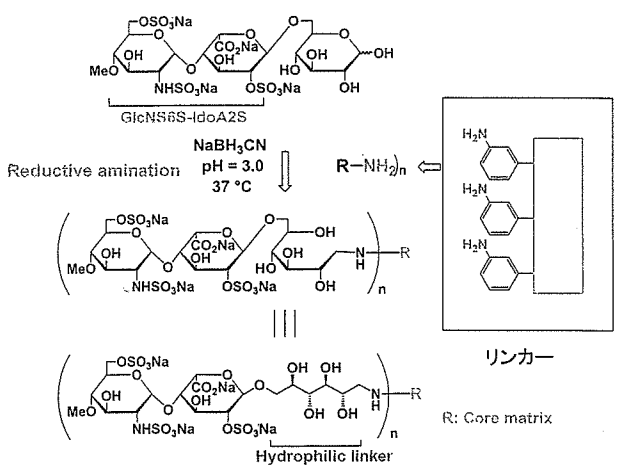

図7　還元アミノ化方法によるオリゴ糖鎖の集合化

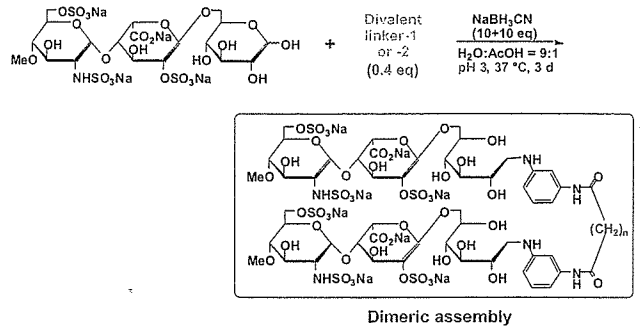

n = 2: 60% (based on linker), ESI-MS (Neg.) m/z = 903.23 [$(M-8Na+6H)^{2-}$]
n = 5: 60% (based on linker), ESI-MS (Neg.) m/z = 924.24 [$(M-8Na+6H)^{2-}$]

図8　図6のストラテジーに基づく集合化オリゴ硫酸化糖鎖の合成例

このようにして、図9に示すように、複数の硫酸化二糖構造を有する一連の構造明確な化合物群を得ることができた。

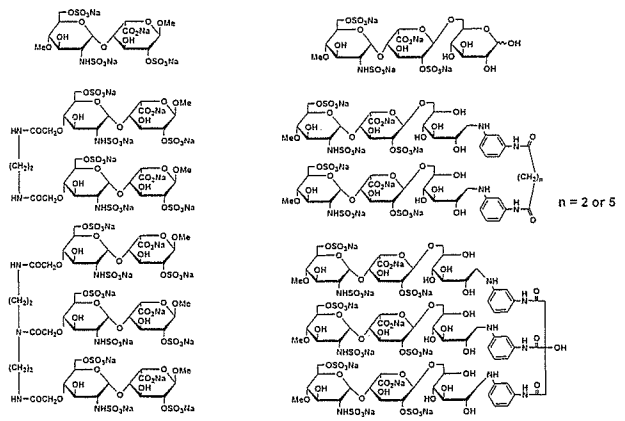

図9　構造明確な集合化オリゴ糖鎖群

そして、血小板への結合挙動を調べたところ、図10に示すように、二糖構造1つだけでは活性を示さない濃度範囲でも、2，3ユニットと増やしていくと活性は明確に存在することが示された。分子量17000程度のヘパリンに比べるとまだ活性は1／500程度にとどまっているが、二糖という非常に小さな単位でも、集合化すれば活性を測定することができることが明確になった。

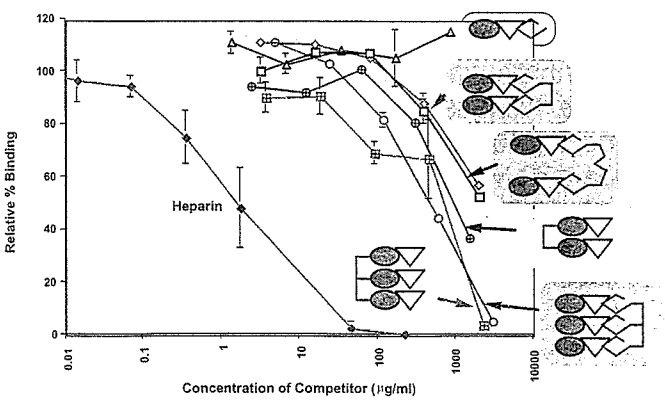

図10　集合化オリゴ糖鎖の血小板結合活性

1．3　ヘパリンとフォンビルブラント因子の結合相互作用の解析

フォンビルブラント因子（vWF）は血小板止血に関与する重要な血液蛋白質であり、血管内皮の損傷部に吸着してそのコンフォメーションが変化すると血小板のGpIbと結合するようになり、結果として血小板を損傷した血管部へ集積させる作用を持つ。しかし、作用のバランスが壊れると血栓症を引き起こすので、特に血管狭窄によって内皮損傷が起こる外科手術後の重篤なトラブルの原因となる。そのため、vWFと血小板GpIbとの結合を阻害する様々な薬剤が開発されているが、ヘパリンにその作用があることがSobelらによって見つけられていた[15]。しかし、ヘパリンをそのまま使うと抗血液凝固作用が大きく、ブリーディング（出血傾向）が起こるので、ヘパリン中の作用部位を特定させ、新規薬剤のリーディング化合物を見つけることは重要であった。

ヘパリンの血小板結合を調べるのと同じ方法を採用した。即ち、ヘパリンをヘパリナーゼまたは過ヨウ素酸とアルカリで低分子化したLMWHを、ヘパリンビーズへのvWFの結合阻害実験と、vWF依存性の血小板凝集阻害実験に供した。図11に示すように、この場合もPI-HepはHI-Hepに比べて高い阻害活性を有していた。即ち、血小板結合と同様に、ヘパリナーゼ消化によって消失する二糖構造GlcNS6S-IdoA2Sが関与することが示唆された[16]。

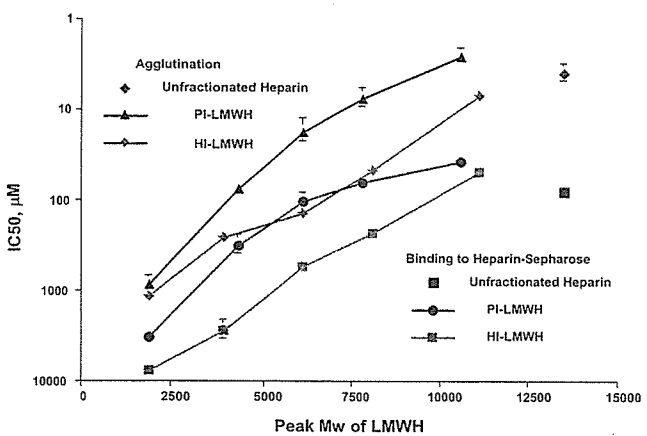

図11　LMWHのvWFに対する結合活性と血小板凝集反応に対する阻害活性

そこで、合成していた集合化化合物を用いて、ヘパリンビーズへのvWFの結合阻害実験を行った。血小板とは異なり、この場合は2単位のGlcNS6S-IdoA2Sでは活性を持たず、3単位持つ化合物でようやく活性が認められた。さらに、血小板とは異なり、3単位でもお互いのユニット間の距離が近い化合物がより高い活性を有した。これらから、ヘパリンのvWF結合にはGlcNS6S-IdoA2Sユニットが3単位以上連結している部分が必要であることが示唆された（図12）。

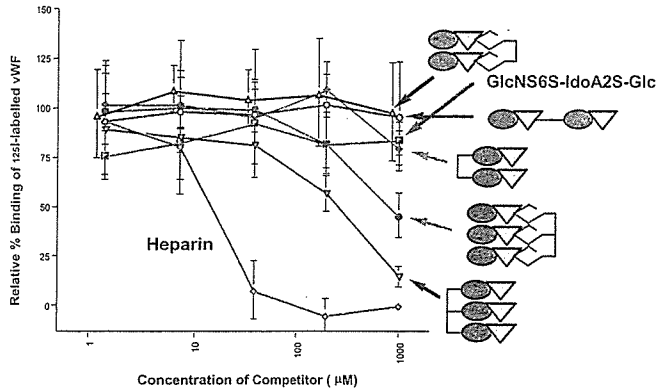

図12　GlcNS6S-IdoA2Sを含む集合化オリゴ糖鎖のvWFへの結合活性

2．シュガーチップの開発[17]

一連のヘパリンの研究から、特定の硫酸化オリゴ糖鎖の活性を調べるためには、それを集合化することが重要であることがわかった。即ち、ヘパリンのような直線性の高分子でも、そのユニットを2次元的に並べれば、活性を評価できる。また、生体内にはムチン糖鎖に代表されるように、オリゴ糖鎖は集合して存在する事が多いことも、集合化を考えなければならない大きな理由である。また、集合化化合物の合成は可能となったが、依然として時間と労力がかかり、構造明確な化合物の量的な不足は常につきまとうこともわかった。これらを解決するために、糖鎖をチップに2次元的に固定し、それを表面プラズモン共鳴（SPR）のセンサーチップに用いることができれば、構造明確なオリゴ糖鎖を複数回使用できるので、量的な問題の解決法の1つになる。また、対象の蛋白質をラジオアイソトープなどで標識することなく、かつリアルタイムで結合挙動を観測できる。さらに、結合相手が不明でも、SPRを用いれば、結合だけは観測できるので、結合を観測した後に質量分析を用いて、蛋白質を同定するというアイデアも生まれた（図13参照）。

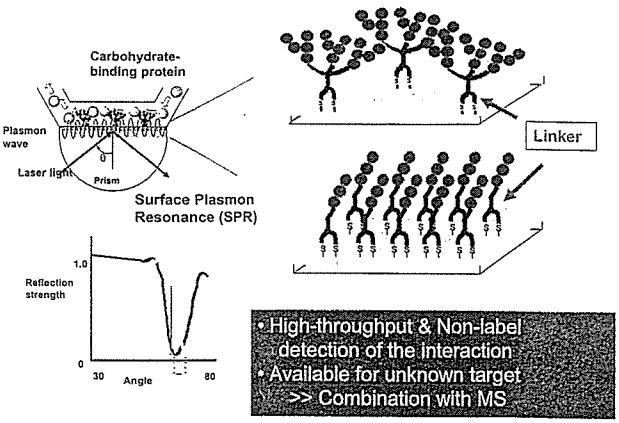

図13　シュガーチップの概念と表面プラズモン共鳴（SPR）

2. 1 疎水性相互作用を利用した糖鎖の固定化

それでは、どのように糖鎖をチップに固定すれば簡単に糖鎖と蛋白質の結合を調べることができるか検討した。もっとも単純、かつ世の中にあった技術としては、チップ上に疎水性の膜を調製しておき、それに疎水化した糖鎖を吸着させるという方法があった。そこで、まずこの方法が適当なものであるか検討するために、図14のように疎水化した硫酸化二糖構造(Hydro-mono-GlcNS6S-IdoA2S-Glc) を合成した。

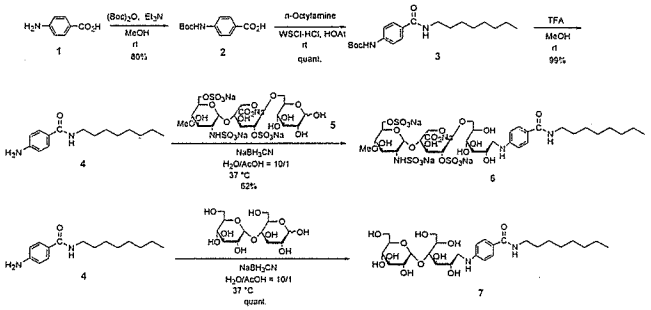

図 14 疎水化硫酸化二糖 (Hydro-mono-GlcNS6S-IdoA2S-Glc) の合成

オクタンチオール基で表面に膜を作製した金チップ[18,19] に、図14 のように合成した Hydro-mono-GlcNS6S-IdoA2S-Glc (Compound 6) を濃度をあげながら添加していくと、SPR のシグナル強度の上昇が見られた。上昇が飽和に達するまで疎水化した二糖構造を添加した後、vWFのヘパリン結合ドメインの合成ペプチド (vWF ーペプチド) を流すとさらに SPR シグナルの上昇が見られた (図 15a)。

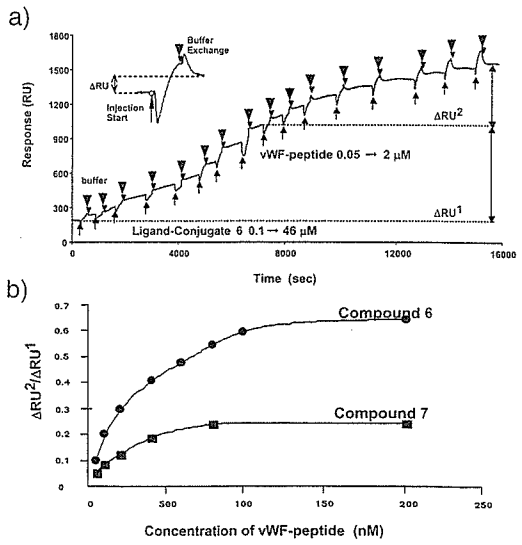

図 15 (a) Hydro-mono-GlcNS6S-IdoA2S-Glc の固定化と vWF ペプチドの結合; (b) 固定した疎水化糖鎖と vWF ペプチドの濃度の関係。Compound 6, 7 は図 14 を参照。

濃度との関係をプロットすると、飽和曲線がかけたので、この方法で糖鎖チップは調製できたと一旦は考えた。しかし、ネガティブコントロールとして用いた疎水化マルトース (Compound 7) を固定化したチップに対しても、vWF ペプチドを流したときに SPR シグナルの上昇が見られた (図 15b)。vWF とαグルコースの結合があるとは思えず、SPR シグナルの上昇は、非特異的相互作用であることが予想された。

これを確かめるために、疎水化マルトースを固定化したチップに BSA を流したところ、非常に大きな SPR シグナルの上昇が見られた。この上昇は、疎水部分への BSA の非特異的吸着と考えられ、この疎水性に基づく固定化は難しいと結論した。

次に、チップ上に固定したアビジンと糖鎖に導入したビオチンとの強い特異的結合を利用した固定化を検討した。これに関しては、別の成書[20] を参考していただきたいが、アビジンに起因する非特異的吸着を避けることはできず、常にネガティブコントロールを同時に測定し、SPR シグナルの差を常に測定する必要があることがわかった。

2. 2 糖鎖固定化の最適

今までの検討から、疎水性の脂質や、アビジンといった物質を介して糖鎖を固定化すると、非特異吸着の問題を避けることができないことがわかった。そこで、糖鎖に金チップに直接結合できる官能基を導入して「糖鎖リガンド複合体」を調製し、それを用いて、糖鎖を固定化することとした。こうすれば、固定化する糖鎖の数 (相対濃度) は比較的簡単にコントロールできるという予想もあった。

糖鎖と金チップをつなぐリンカーとしては、糖鎖の集合化合物を合成する際に有効であった還元アミノ化反応を効率よく進めることができる芳香族アミンと、金と Au-S 結合を作ることができ、かつ分子内環構造を有するチオクト酸を用いることにした。分子内環化SS結合があるため、一時的に還元環境に晒されてSS結合が解離しても、すぐに空気酸化を受けて元の構造に戻ることが予想され、糖鎖リガンド複合体を精製する際に手間取らないと考えたこともチオクト酸を採用した理由である。図 16 に示したように、末端にグルコースを導入したヘパリン部分二糖構造 (GlcNS6S-IdoA2S-Glc)をまず完成させた後、リンカーを反応さ

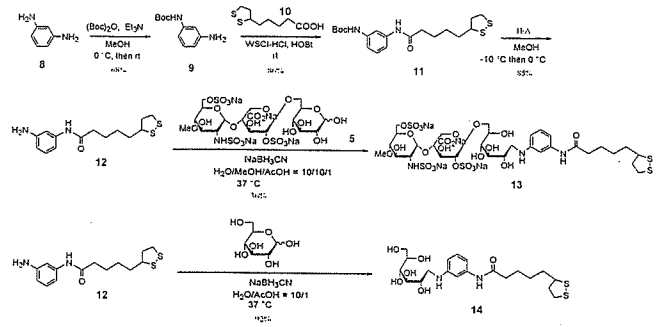

図 16 Mono-valent 型糖鎖リガンド複合体の合成

せ、60%以上の収率でリガンド複合体、Mono-GlcNS6S-IdoA2S-Glcを得た。前述したように、末端のグルコースは親水性のリンカーとしても機能し、糖鎖を金チップから離して、蛋白質の結合を容易にすること、また疎水性に基づく非特異吸着を最小限にすることを期待した。

合成したリガンド複合体Mono-GlcNS6S-IdoA2S-Glc (Compound 13) を50%メタノール溶液で10 μMに調製し、その溶液にSPRの金チップを浸せきし、室温で終夜反応させ、固定化チップを調製した。これに2 μMのvWFペプチドを流したところ、標準的なSPRセンサグラムが得られた（図17a)。一方、疎水性を利用した固定化法では非常に大きなSPRシグナルと、バッファーで洗浄してもチップ上に吸着したままだったBSAを流した場合には、かなりの高濃度の溶液を流した場合でも、非常に小さなSPRシグナルしか観測されず、またバッファーの洗浄後速やかにベースラインに戻ったことから、このチップにはBSAはほとんど結合しないことが示された。即ち、糖鎖をこの方法で金チップに直接結合させることによって、非特異的吸着をほぼ無視できる系を構築することができた。vWFペプチドを結合させた後、800秒間バッファーで洗浄しても残っているSPRシグナル量を平衡結合量(equilibrium binding) とし、vWFの濃度に対してプロットすると、図17bが得られた。この図からKD値を210 nMと推定した。この値は、ラジオアイソトープラベルしたヘパリンを用いて得られた報告値 (370±200 nM) [21]と大差なかった。比較対照として、グルコースにリンカーを導入したリガンド複合体(Mono-Glc, Compound 14)を用いて、同様の実験を行った。この際vWFペプチドの濃度を上げても、全くSPRシグナルの上昇は見られず、非特異的吸着を無視できる系であることが確認された（図17b)。

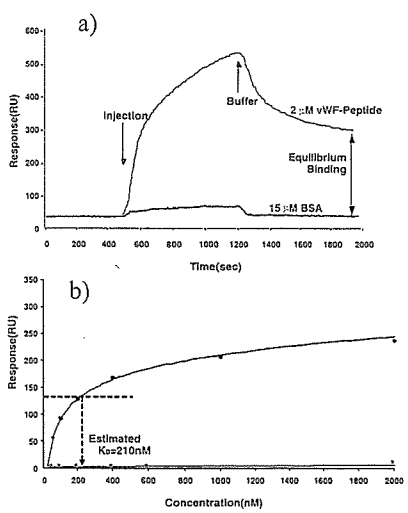

図17 (a) Mono-GlcNS6S-IdoA2S-Glcを固定化したチップへのvWFペプチドおよびBSAの結合挙動。(b)vWFペプチドのMono-GlcNS6S-IdoA2S0Glcおよび Mono-Glcを固定化したチップへの結合。

このチップを用いて、vWFのヘパリン結合ドメインを含む部分リコンビナント蛋白質(vWF-A1)[22,23]の結合挙動を観測した。蛋白質濃度の上昇にともなってSPRシグナルの上昇が見られ、KD値は1.2 μMと推定できた。

2. 3 クラスター化の検討

このように、モノバレントのリガンド複合体を用いて、糖鎖と糖鎖結合性の蛋白質の結合挙動をリアルタイムで測定することができるようになった。この場合、リガンドの固定化は容易であり、チップ上にリガンドはほぼ均一に分散していると考えられるが、糖鎖クラスターの密度（オリゴ糖鎖のチップ表面の濃度）はリガンド複合体溶液の濃度や金チップの状態（凹凸）に依存する。それらに依存しない系を構築するために、複数ユニットのオリゴ糖鎖が常に2～5nmの距離内に集合した状態でチップ上に固定化されたMulti-valent型のリガンド複合体について次に検討した。

2. 3. 1 合成

Ashtonらの報告[24]を参考にして、Tri- およびTetra-valentリンカーとリガンド複合体の合成を図18,19のように行い、それぞれTri-GlcNS6S-IdoA2S-Glc、Tetra-GlcNS6S-IdoA2S-Glc-longを合成した。この過程で、集合化する糖鎖の大きさにもよるが、集合化する糖鎖の数が多くなるに従い、リンカー中のSS部位が金チップ表面に接触しにくくなるという立体反発的な要素が大きくなる事がわかった。そのため、分岐部分とチオクト酸部分の間のスペーサーを長くする必要があった。この際、疎水性を高めないためにオリゴエチレングリコールの利用が効果的であった。

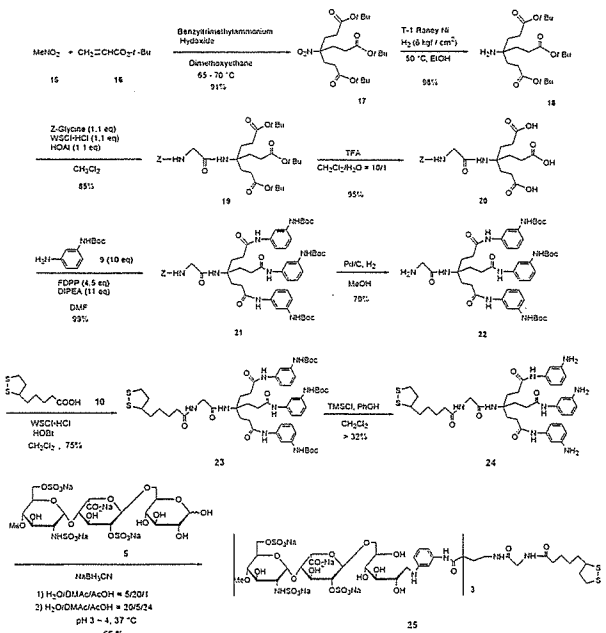

図18 Tri-GlcNS6S-IdoA2S-Glcの合成

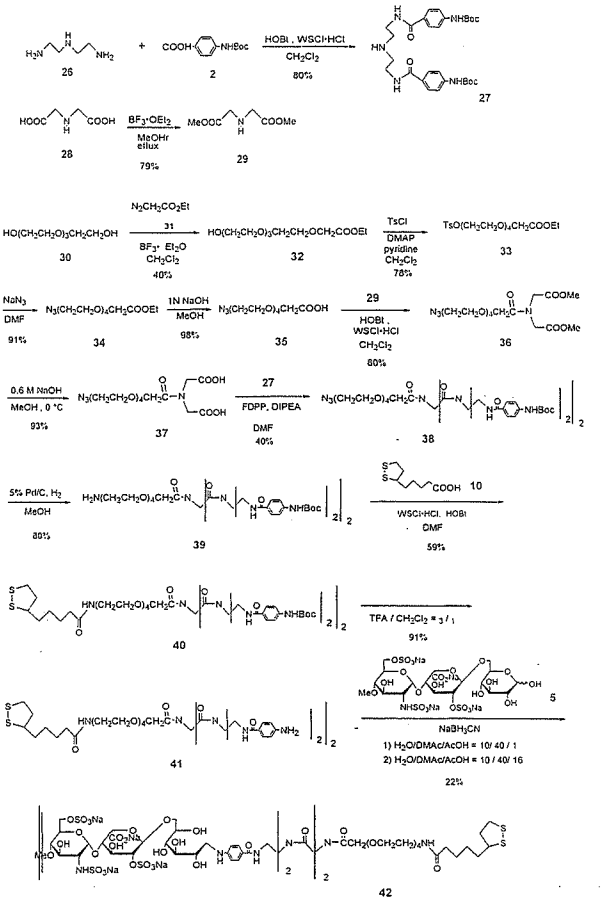

図19　Tetra-GlcNS6S-IdoA2S-Glc-longの合成

2. 3. 2　クラスター化リガンド複合体を用いた結合活性の評価

Tri-GlcNS6S-IdoA2S-Glc (Compound 25)およびTetra-GlcNS6S-IdoA2S-Glc-long (Compound 42) を固定化したチップへ1.5 μM のBSAを流した時には、Mono- GlcNS6S-IdoA2S-Glcを固定化したチップと同様（図17）、SPRシグナルは僅かに上昇するが、バッファーで洗うと直ちにベースラインに戻り、BSAはこのチップにはほとんど結合しない、即ち非特異吸着は無視できることが分った。

このように、直接結合型のリンカーを用いて糖鎖を金チップに固定化すると、非特異吸着は無視できることが明らかとなったので、次に固定化された糖鎖リガンドの密度の影響を検討した。即ち、硫酸化二糖構造をもつMon-, Tri-, およびTetra-valent リガンド複合体と、糖鎖構造をもたないMono-Glc (Compound 8)を混合した溶液を先ず調製し、それに金チップを浸漬することによってチップ上の相対リガンド濃度が違うチップを調製した。

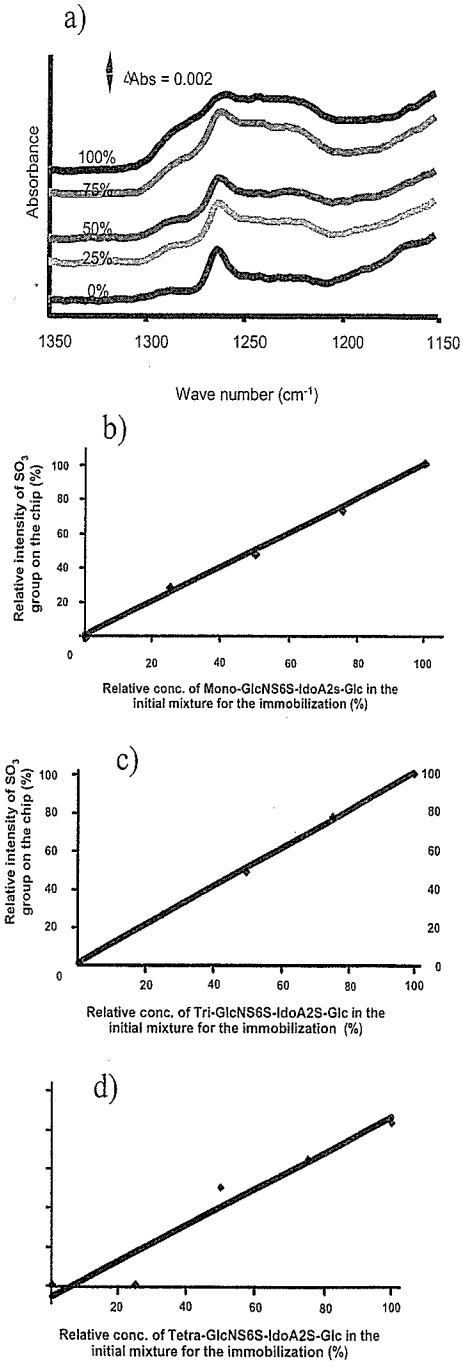

図20　(a) Mono-GlcNS6S-IdoA2S-GlcとMono-Glcを混合して作成したチップのATR-FT-IRスペクトル。(b) Mono-GlcNS6S-IdoA2S-GlcとMono-Glcの仕込み比とチップ上の硫酸基の相対強度との関係（R^2 = 0.9984）。(c) Tri-GlcNS6S-IdoA2S-GlcとMono-Glcの仕込み比とチップ上の硫酸基の相対強度との関係（R^2 = 0.9993）。(d) Tetra-GlcNS6S-IdoA2S-Glc-longとMono-Glcの仕込み比とチップ上の硫酸基の相対強度との関係（R^2 = 0.9610）。

相対濃度は、各々のチップをATR-FT-IRで測定し、1200 から 1303 cm^{-1} に現れる硫酸基の吸収を積分して定量した。図20aにMono-GlcNS6S0IdoA2S-GlcとMono-Glcをそれぞれ混合比を変えて作成したチップのATR-FT-IRスペクトルを、20b-20dには相対濃度と、仕込み比の関係を示した。
いずれの場合も、仕込み比と相対濃度には直線関係が成り立っており、硫酸化二糖はチップ上で均一に分散して固定化されていることが示唆された。また、仕込み比を変えることでチップ上の硫酸化二糖構造の相対濃度を調整できることも明らかとなった。

2. 3. 3 ヘパリン結合性蛋白質の結合親和性

リコンビナントのヒトvWf-A1 domain (rhvWf-A1)[22,23]をモデル蛋白質に用いて、3つのリガンド複合体について、チップ上の糖鎖の密度（100% と 50%）と結合親和性の相関について検討し、表1に結果をまとめた。

表1　rhvWf-A1の結合挙動：チップに固定化された硫酸化二糖構造のクラスター効果

Ligand-conjugates	ratio	K_D (μM)	k_a ($M^{-1}s^{-1}X10^3$)	k_d ($s^{-1}X10^{-3}$)
Mono-GlcNS6S-IdoA2S-Glc / Mono-Glc	100 / 0	2.60	8.38	21.9
	50 / 50	3.79	14.6	55.2
Tri-GlcNS6S-IdoA2S-Glc / Mono-Glc	100 / 0	1.20	6.60	8.05
	50 / 50	1.50	4.52	6.83
Tetra-GlcNS6S-IdoA2S-Glc / Mono-Glc-long	100 / 0	0.99	6.50	6.44
	50 / 50	1.00	5.24	5.26

$K_D = k_d / k_a$ (Dissociation Constant)
k_a : association rate
k_d : dissociation rate

リガンド複合体中の硫酸化二糖構造の数が増えていくにつれて、小さなKD（高い親和性）を有することが明確になっている。Mono-valentリガンド複合体と比べると、その親和性は3倍程度高い。この理由は、解離速度定数 k_d が小さいことから、クラスター化されたリガンドの場合は数 nm 以内に糖鎖が存在しているため、結合と解離の平衡にあるとき、解離した蛋白質がすぐ近くのリガンドに再び結合することが出来、その結果ネットの解離速度定数が小さくなっていると解釈できる。リガンド複合体の濃度を50%に低下させると、クラスター化リガンドの効果はさらに明確になった。即ち、Tri-valentやTetra-valentのリガンド複合体はKDの値はほとんど変わらなかったが、Mono-valentリガンド複合体ではKDは1.5倍になっていた。

次に、部分構造ではなく全ヒトvWF蛋白質について検討した。この蛋白質は単量体でも分子質量が270 kDaもある巨大な蛋白質であるだけではなく、自己会合性が高く、一般に溶液中で存在しているときはその分子量は数百万におよび、また会合に伴いヘパリン結合ドメインも複数有している。3種類のリガンド複合体の濃度をそれぞれ100%と20%に変化させて調製したチップを用いてvWFの結合活性を調べ、表2に結果をまとめた。

表2　whole rhvWFの結合挙動：チップに固定化された硫酸化二糖構造のクラスター効果が見られない例

Ligand-conjugates	Ratio	Estimated K_D (nM)
Mono-GlcNS6S-IdoA2A-Glc / Mono-Glc	100 / 0	35
	20 / 80	41
Tri-GlcNS6S-IdoA2A-Glc / Mono-Glc	100 / 0	24
	20 / 80	27
Tetra-GlcNS6S-IdoA2A-Glc / Mono-Glc-long	100 / 0	35
	20 / 80	32

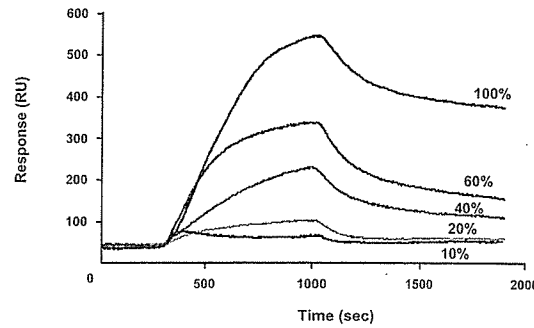

図21　Mono-GlcNS6S-IdoA2Sを固定化したチップ上のリガンドの相対密度のvWFペプチド（2 μM）の結合に与える影響。

先の表1の結果とは異なり、推定したKD値は全てほぼ同じであった。全vWF蛋白質の場合は会合してヘパリン結合ドメインが複数あるため、チップ上の硫酸化二糖の密度の影響がほとんどないのであろう。

なお、vWF-ペプチドとMono-valentリガンドの結合を調べると、相対密度が40%以上ないと結合が見られなかった（図21）。

これらから、チップ上の糖鎖の相対密度、またリガンドのMulti-valencyを変化させて結合相互作用を評価することによって、蛋白質の糖鎖結合ドメインがシングルかマルチかという判断をすることも出来ることが示された。

最後に、調製した硫酸化二糖構造を固定化したチップを用いて、結合阻害実験を行ってみた。すなわち、チップはTri-GlcNS6S-IdoA2S-Glcを固定化して調製し、200 nMのbFGF（塩基性繊維芽細胞増殖因子）と阻害剤としてヘパリンを濃度を変えて加え、そのときのSPRシグナルの変化を測定した。図22(a)にはSPRシグナルの変化を、図22(b)には阻害剤のヘパリン（平均分子量15000）の濃度と、結合したbFGFの濃度をプロットした。図22(b)から、ヘパリンの阻害濃度IC50は50-100 nMであると見積もることが出来た。なお、この値はbFGFのヘパラン硫酸プロテオグリカンへのKD値[25]と近いものであり、この方法の有用性が示唆された。

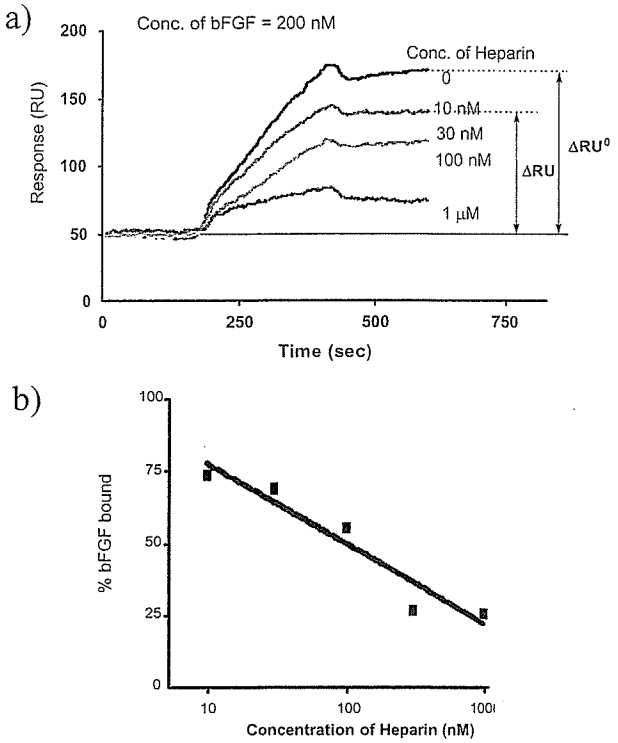

図22　硫酸化二糖構造を固定化したチップを用いたbFGFの結合に対するヘパリンの阻害実験 (a) SPR センサーグラム、(b) ヘパリン濃度とbFGFの結合に起因するSPRシグナルの増加度

3. 結語

ヘパリンと血小板、またvWFとの相互作用を、構造明確なオリゴ糖鎖を用いることによって、分子レベルでの解析を行うという目的で始めた研究が、糖鎖固定化チップ（他との差別化のために、シュガーチップと総称している）の開発に繋がった。現在では、リガンド複合体の数も70種類程度にのぼり、糖鎖と結合する蛋白質をSPR法で系統的に解析したデータベースも整備することが出来た。また、シュガーチップを調製する技術を金ナノ粒子に応用し、糖鎖固定化金ナノ粒子（SGNPと総称）の開発にも成功した[26]。SGNPは高価なSPR測定機器を用いることなく、糖鎖と蛋白質の相互作用を可視で判断できるものである。そして、研究成果の社会還元を目指し、本年9月に起業し、シュガーチップを用いた受託研究やSGNPの販売を行うことが出来るようになった[27]。なお、糖鎖チップや糖鎖アレイの技術は、世界中で開発されている[28-33]。しかし、そのほとんどは、対象とする蛋白質をあらかじめ蛍光色素や酵素で標識するか、結合後に抗体を組み合わせて蛋白質が結合した糖鎖を同定するものであり、SPRと組み合わせることで網羅的な解析を可能とする技術はわれわれ以外にはほとんど報告がないことを追記する。

わが国の糖鎖研究は世界をリードする立場を保っている。我々の技術が、わが国の糖鎖研究の国際優位性を保つのに役立つこと、さらに現在開発研究を進めているシュガーチップ技術を用いた各種疾患の検査・診断技術の開発を通じて、世界人類に貢献したいと考えている。

4. 謝辞

本研究は、筆者の前任地の大阪大学大学院理学研究科楠本研究室で開始し、鹿児島大学で確立させることが出来たものであり、日本学術振興会の重点領域研究（代表者、楠本正一大阪大学教授、現㈶サントリー生物有機科学研究所長）、(独) 科学技術振興機構の権利化試験事業およびプレベンチャー事業（代表者：筆者）のサポートを受けた。文中にも述べたが、現ワシントン大学医学部のSobel教授は、この研究を開始したときからの共同研究者である。また、化合物の合成やSPR実験では、大学院生であった市山君（現、大日本住友製薬）、越田君（現、北海道大学助手）、荒野君（現、東亞合成化学）をはじめとして、多くの方々のサポートを頂いた。ここに深く感謝します。また、本稿の執筆の機会を与えて下さった㈱同仁化学研究所の関係各位に深謝します。

参考文献

1) *Heparin,* (1989) (Eds.: Lane, D. A. and Lindahl, U.), CRC Press Inc., Boca Raton, FL, and references therein.
2) Esko, J. D. (1999) in *Essentials of Glycobiology,* (Eds.: Varki, A., Cummings, R., Esko, J., Freeze, H., Hart, G., and Marth, J.), Cold Spring Harbor Laboratory Press, Cold Spring Harbor, New York, NY, pp. 441-453, and references therein.
3) Gallagher, J. (2001) Heparan sulfate: growth control with a restricted sequence menu. *J. Clinic. Invest. 108*, 357.
4) Ostrovsky, O., Berman, B., Gallagher, J., Mulloy, B., Fernig, D. G., Delehedde, M., and Ron, D. (2001) Differential effects of heparin saccharides on the formation of specific fibroblast growth factor (FGF) and FGF receptor complexes. *J. Biol. Chem. 277*, 2444.
5) Faham, S., Hileman, R. E., Fromm, J. R., Linhardt, R. J., Rees, D. C. (1996) Heparin structure and interactions with basic fibroblast growth factor. *Science 271*, 1116.
6) Choay, J., Lormeau, J. -C., Petitou, M., Sinay, P. and Fareed, J. (1981) Structural studies on a biologically active hexasaccharide obtained from heparin. *Ann. New York Acad. Sci., 370*, 644.
7) Thunberg, L., Backstrom, G. and Lindahl, U. (1982) Further characterization of the antithrombin-binding sequence in heparin. *Carbohydr. Res., 100*, 393.
8) Salzman, E. W., Rosenberg, R. D., Smith, M. H., Lindon, J. N. and Favreau, L. (1980) Effect of heparin and heparin fractions on platelet aggregation. *J. Clin. Invest., 65*, 64.
9) Suda, Y., Marques, D., Kermode, J. C., Kusumoto, S. and Sobel, M. (1993) Structural characterization of heparin's binding domain for human platelets. *Thromb. Res., 69*, 501.

10) Sobel, M., Ottenbrite, R. M. and Suda, Y. (1991) Fluorescent labeling of heparins and related polysaccharides: Old problems and new solutions, in:Polymeric Drugs and Drug Delivery systems (Eds.: Dunn, R. L. and Ottenbrite, R. M.), ACS Symposium Series *469*, American Chemical Society, Washington D. C., pp. 60.
11) Suda, Y., Bird, K., Shiyama, T., Koshida, S., Marques, D., Fukase, K., Sobel, M. and Kusumoto, S. (1996) Synthesis and biological activity of a model disaccharide containing a key unit in heparin for binding to platelets, *Tetrahedron Lett.*, 37, 1053.
12) Koshida, S., Suda, Y., Fukui, Y., Ormsby, J., Sobel, M., and Kusumoto, S. (1999) Synthesis and biological activity of oligomer-model compounds containing units of a key platelet-binding disaccharide of heparin. *Tetrahedron Lett. 40* (21), 5725.
13) Koshida, S., Suda, Y., Arano A., Sobel, M., and Kusumoto, S. (2001) An efficient method for the assembly of sulfated oligosaccharides using reductive amination. *Tetrahedron Lett. 42 (7)*, 1293.
14) Koshida, S., Suda, Y., Sobel, M., and Kusumoto, S. (2001) Synthesis of oligomeric assemblies of a platelet-binding key disaccharide in heparin and their biological activities. *Tetrahedron Lett. 42 (7)*, 1289.
15) Sobel, M., McNeill, P. M., Carlson, P.L., Kermode, J. C., Adelman, B., Conroy, R. and Marques, D. (1991) Heparin inhibition of von Willebrand factor-dependent platelet function in vitro and in vivo. *J Clin Invest., 87*, 1787.
16) Poletti, L. F., Bird, K. E., Marques, D., Harris, R. B., Suda, Y., and Sobel, M. (1997) Structural aspects of heparin responsible for interactions with von Willebrand factor. *Arterioscler. Thromb. Vasc. Biol. 17* (5), 925.
17) Suda, Y., Arano, A., Fukui, Y., Koshida, S., Wakao, M., Nishimura, T., Kusumoto, S. and Sobel, M. (2006) Immobilization and clustering of structurally defined oligosaccharides for sugar chips: an improved method for surface plasmon resonance analysis of protein-carbohydrate interactions. *Bioconjug Chem., 17*, 1125.
18) Peterlinz, K. A., and Georgiadis, R. (1996) In situ kinetics of self-assembly by surface plasmon resonance spectroscopy. *Langmuir 12* (20), 4731.
19) Liedberg, B., Nylander, C., and Lundströ, I. (1983) Surface plasmon resonance for gas detection and biosensing. *Sensors and Actuators 4*, 299.
20) 隅田泰生 ”糖鎖チップ“ (2005) 糖鎖科学の新展開 - 機能解明・次世代型材料・医薬品開発に向けて（谷口直之、伊藤幸成 編）エヌティーエヌ、pp. 471.
21) Sobel, M., Soler, D. F., Kermode, J. C., and Harris, R. B. (1992) Localization and characterization of a heparin binding domain peptide of human von Willebrand factor. *J. Biol. Chem. 267*, 8857.
22) Cruz, M. A., Handin, R. I., Wise, R. J. (1993) The Interaction of the von Willebrand Factor A1 Domain with Platelet Glycoprotein Ib Ix – The role of glycosylation and disulfide bonding in a monomeric recombinant A1 domain protein. *J. Biol. Chem.* 1993, *268*, 21238.
23) Rastegar-Lari, G., Villoutreix, B. O., Ribba, A.S., Legendre, P., Meyer, D., and Baruch, D. (2002) Two clusters of charged residues located in the electropositive face of the von Willebrand factor A1 domain are essential for heparin binding. *Biochemistry 41*, 6668.
24) Ashton, P. R., Boyd, S. E., Brown, C. L., Nepogodiev, S. A., Meijer, E. W., Peerlings, H. W. I., and Stoddart, J. E. (1997) Synthesis of glycodndrimers by modification of poly(propylene imine) dendrimers. *Chemistry-A Eur. J. 3*, 974.
25) Presta, M., Maier, J. A., Rusnati, M., and Ragnotti, G. (1989) Basic fibroblast growth factor is released from endothelial extracellular matrix in a biologically active form. *J. Cell. Physiol. 140,* 68.
26) Suda, Y., Kishimoto, Y., Nishimura, T., Yamashita, S., Hamamatsu, M., Saito, A., Sato, M., and Wakao, M (2006) Sugar-immobilized gold nano-particles (SGNP): Novel bioprobe for the on-site analysis of the oligosaccharide protein interactions, *Polymer Preprints* **47**(2), 156.
27) URL http://www.sudxbiotec.jp/
28) Houseman, B. T., and Mrksich, M. (2002) Carbohydrate arrays for the evaluation of protein binding and enzymatic modification. *Chem. Biol. 9*, 443.
29) Fazio, F., Bryan, M. C., Blixt, O., Paulson, J. C., and Wong, C. -H. (2002) Synthesis of sugar arrays in microtiter plate. *J. Am. Chem. Soc. 124* (48), 14397.
30) Park, S., Lee, M. -R., Pyo, S. -J., and Shin, I. (2002) Carbohydrate chips for studying high-throughput carbohydrate-protein interactions. *J. Am. Chem. Soc. 126* (15), 4812.
31) Ratner, D. M., Adams, E. W., Su, J., O'Keefe, B. R., Mrksich, M., and Seeberger, P. H. (2004) Probing protein–carbohydrate interactions with microarrays of synthetic oligosaccharides. *ChemBioChem. 5*, 379.
32) de Paz, J. L., Noti, C., and Seeberger P. H. (2006) Microarrays of synthetic heparin oligosaccharides. *J. Am. Chem. Soc., 128,* 2766.
33) Feizi, T., and Chai, W. (2004) Oligosaccharide microarrays to decipher the glyco code. *Nature Reviews, 5*, 582.

筆者紹介
氏　　名：隅田 泰生
所　　属：鹿児島大学大学院理工学研究科
　　ナノ構造先端材料工学専攻
連 絡 先：〒890-0065 鹿児島県鹿児島市郡元 1-21-40
出身大学：大阪大学大学院工学研究科
研究テーマ：糖鎖生物化学に関する研究
専門分野：糖鎖生化学、ナノテクノロジー

Journal of Neurochemistry, 2006, **99**, 198–205 doi:10.1111/j.1471-4159.2006.04035.x

Styrylbenzoazole derivatives for imaging of prion plaques and treatment of transmissible spongiform encephalopathies

Kensuke Ishikawa,* Yukitsuka Kudo,† Noriyuki Nishida,‡ Takahiro Suemoto,§ Tohru Sawada,§ Toru Iwaki¶ and Katsumi Doh-ura*

**Department of Prion Research, Tohoku University Graduate School of Medicine, Sendai, Japan*

†Division of Telecommunication and Information Technology, Biomedical Engineering Research Organization, Tohoku University, Sendai, Japan

‡Division of Cellular and Molecular Biology, Nagasaki University Graduate School of Biomedical Sciences, Nagasaki, Japan

§BF Research Institute Inc., Osaka, Japan

¶Department of Neuropathology, Graduate School of Medical Sciences, Kyushu University, Fukuoka, Japan

Abstract

Recent prevalence of acquired forms of transmissible spongiform encephalopathies (TSEs) has urged the development of early diagnostic measures as well as therapeutic interventions. To extend our previous findings on the value of amyloid imaging probes for these purposes, styrylbenzoazole derivatives with better permeability of blood–brain barrier (BBB) were developed and analyzed in this study. The new styrylbenzoazole compounds clearly labeled prion protein (PrP) plaques in brain specimens from human TSE in a manner irrespective of pathogen strain, and a representative compound BF-168 detected abnormal PrP aggregates in the brain of TSE-infected mice when the probe was injected intravenously. On the other hand, most of the compounds inhibited abnormal PrP formation in TSE-infected cells with IC_{50} values in the nanomolar range, indicating that they represent one of the most potent classes of inhibitor ever reported. BF-168 prolonged the lives of mice infected intracerebrally with TSE when the compound was given intravenously at the preclinical stage. The new compounds, however, failed to detect synaptic PrP deposition and to show pathogen-independent therapeutic efficacy, similar to the amyloid imaging probes we previously reported. The compounds were BBB permeable and non-toxic at doses for imaging and treatment; therefore, they are expected to be of practical use in human TSE.

Keywords: amyloid imaging, anti-prion activity, pathogen strain, prion disease, styrylbenzoazole derivatives.

J. Neurochem. (2006) **99**, 198–205.

The transmissible spongiform encephalopathies (TSEs) or prion diseases form a group of neurodegenerative disorders characterized by abnormal deposition of protease-resistant isoforms of prion protein (PrP) in the CNS (Prusiner 1991). TSEs are classified as sporadic, hereditary or environmentally acquired, and have become a serious public health issue because of the recent prevalence of acquired Creutzfeldt–Jakob disease (CJD), such as the variant form due to bovine spongiform encephalopathy (Will *et al.* 1996) and the iatrogenic form with cadaveric growth hormone or dura grafts (Brown *et al.* 2000). There is an urgent need to develop prophylactic and therapeutic interventions as well as diagnostic measures at the preclinical or early clinical stages of these incurable diseases.

We have previously reported that some amyloid imaging compounds, primarily derived from amyloid dyes such as

Received February 16, 2006; revised manuscript received May 25, 2006; accepted May 30, 2006.

Address correspondence and reprint requests to Dr Kensuke Ishikawa, Division of Prion Biology, Department of Prion Research, Tohoku University Graduate School of Medicine, 2–1 Seiryo-machi, Aoba-ku, Sendai 980-8575, Japan. E-mail: ishikawa@mail.tains.tohoku.ac.jp

Abbreviations used: AD, Alzheimer's disease; BBB, blood–brain barrier; BSB, (trans, trans)-1-bromo-2,5-bis-(3-hydroxycarbonyl-4-hydroxy)styrylbenzene; CJD, Creutzfeldt–Jakob disease; DMSO, dimethylsulfoxide; FDDNP, 2-(1-[6-[(2-fluoroethyl)(methyl)amino]-2-naphthyl]ethylidene)malononitrile; GSS, Gerstmann–Strässler–Scheinker syndrome; ICR, Institute of Cancer Research; ID, injected dose; NT, not tested; PrP, prion protein; PrPres, protease-resistant PrP; PTA, phosphotungstic acid; PVDF, polyvinylidene difluoride; TSE, transmissible spongiform encephalopathy.

Congo red and thioflavin T, are useful for detection of prion plaques and treatment of TSE (Ishikawa *et al.* 2004). These compounds, however, are limited in their ability because of inefficient brain uptake. Here we describe new compounds, styrylbenzoazole derivatives, which have been developed for practical use and analyzed for their PrP imaging ability, anti-prion activity, therapeutic efficacy, brain uptake and toxicity.

Materials and methods

Chemicals and experimental models

All of the test compounds were synthesized at Tanabe R & D (Saitama, Japan) and used freshly after being dissolved in 100% dimethylsulfoxide (DMSO).

Cultured cells were grown in Opti-MEM (Invitrogen, Carlsbad, CA, USA) supplemented with 10% fetal calf serum. As cellular models of TSE, we used mouse neuroblastoma (N2a) cells persistently infected with the RML strain (ScN2a) (Race *et al.* 1988) and six other prion-infected cell lines: N2a58 cells individually infected with the RML strain, the 22L strain (Nishida *et al.* 2000) and Fukuoka-1 strain (Ishikawa *et al.* 2004); N2a cells infected with the 22L strain; mouse hypothalamic cells (GT1-7) infected with the 22L strain (Milhavet *et al.* 2000); and mouse fibroblast cells (L929) infected with the RML strain (Vorberg *et al.* 2004).

Tg7 mice overexpressing hamster PrP (Race *et al.* 1995) and Tga20 mice overexpressing mouse PrP (Fischer *et al.* 1996) were also used. These mouse models were intracerebrally infected with 20 μL brain homogenate comprising 1% (w/v) of the 263K strain and the RML strain respectively. The Tg7 mice showed plaque-type PrP deposition between the cerebral cortex and hippocampus by 6 weeks after infection, followed by synaptic-type PrP deposition in the thalamus. The Tga20 mice showed similar pathological deposition, but plaques were not seen as frequently. Each mouse weighed ~30 g, and was maintained under deep ether anesthesia for minimum distress during all surgical procedures. Permission for the animal study was obtained from either the Animal Experiment Committee of Kyushu University or Tohoku University, Japan.

Brain uptake study

Test compounds were administered intravenously to Institute of Cancer Research (ICR) mice under ether anesthesia to determine initial brain uptakes. At 2 or 30 min after injection, the brains were removed, weighed and homogenized with saline. After centrifugation of the homogenate at 21 900 *g* for 10 min, the supernatant was applied to a conditioned C18 solid-phase extraction cartridge, and the compounds were eluted with methyl alcohol. Fluorescence was detected by high performance liquid chromatography with a fluorescence detector as reported previously (Okamura *et al.* 2005), and the percentage of injected dose per gram (%ID/g) was used as a measure of the level of the compounds in the brain.

In vitro PrP imaging in sections

Autopsy-diagnosed brain samples from cases of Gerstmann–Strässler–Scheinker syndrome (GSS) ($n = 2$), sporadic CJD ($n = 5$), iatrogenic dura CJD with synaptic PrP deposition ($n = 1$) and non-TSE control cases with amyloid lesions [Alzheimer's disease (AD), $n = 2$] or without amyloid lesions (cerebral infarction, $n = 1$) were obtained from the Department of Neuropathology, Kyushu University, Japan. After fixation in 10% buffered formalin for 2 weeks, each sample of TSE was immersed in 98% formic acid for the reduction of prion infectivity, embedded in paraffin and cut into sections 7 μm thick. Sections of a variant CJD case were kindly provided by Dr James W. Ironside of the CJD Surveillance Unit, Edinburgh, UK. For neuropathological staining, deparaffinized sections were immersed in 1% Sudan black solution to quench tissue autofluorescence. They were then incubated for 30 min in 1-μM solutions of the test compounds, rinsed with distilled water and examined under a fluorescence microscope (DMRXA; Leica Instruments, Wetzler, Germany) with a UV or FITC filter set.

For comparison, each section was subsequently immunoassayed for PrP as described previously (Doh-ura *et al.* 2000). Briefly, the sections were treated with a hydrolytic autoclave and incubated with a rabbit primary antibody, c-PrP, which was raised against a mouse PrP fragment, amino acids 214–228 (1 : 200; Immuno-Biological Laboratories, Gunma, Japan), followed by incubation with a horseradish peroxidase-conjugated secondary antibody (1 : 200; Vector Laboratories, Burlingame, CA, USA). The reaction product was developed with 3,3′-diaminobenzidine tetrahydrochloride solution and counterstained with hematoxylin. Paraffin-embedded brains of experimental animals were similarly investigated.

In vivo PrP imaging in model animals

BF-168 (molecular weight 312.34) dissolved in 10% DMSO was administered intravenously (0.5–5 mg/kg body weight) into Tg7 mice at 6–7 weeks after injection when the mice showed no apparent clinical signs of TSE. As controls, vehicle alone was similarly injected into infected mice, and BF-168 was administered into uninfected mice. The animals were killed at various time points, and the brains were rapidly frozen and cut into coronal sections 10 μm thick using a cryostat (CM3050; Leica Instruments). The sections were thaw-mounted on slides, dried and coverslipped. They were examined under a fluorescence microscope and further analyzed immunohistochemically as described above.

In vitro treatment in cell cultures

Abnormal PrP formation was assayed by the content of protease-resistant PrP (PrPres) in cellular models of TSE as described previously (Caughey and Raymond 1993). Each compound was added at the designated concentrations when cells were passaged at 10% confluence, while maintaining the final concentration of DMSO in the medium at < 0.5%. The cells were allowed to grow to confluence and lysed with lysis buffer (0.5% sodium deoxycholate, 0.5% Nonidet P-40, phosphate-buffered saline). For analysis of PrPres, samples were digested with 10 μg/mL proteinase K for 30 min, and the digestion was stopped with 0.5 mM phenylmethylsulfonyl fluoride. The samples were centrifuged at 100 000 *g* for 30 min, and pellets were resuspended in 1 × sample loading buffer and boiled. For analysis of cellular PrP in N2a cells, cell lysates were mixed directly with a quarter volume of 5 × sample loading buffer and boiled. These samples were separated by electrophoresis on a 15% Tris–glycine–sodium dodecyl sulfate polyacrylamide gel and electroblotted on to a polyvinylidene difluoride (PVDF) filter (Millipore, Bedford, MA, USA). PrP was detected using a monoclonal antibody, SAF83 (1 : 5000; SPI-BIO, Massy, France), followed by an alkaline phosphatase-conjugated

goat anti-mouse antibody (1 : 20 000; Promega, Madison, WI, USA). Immunoreactive blots were visualized with CDP-Star detection reagent (Amersham, Piscataway, NJ, USA). More than two independent assays were performed in each experiment and signals were analyzed using image analysis software. The approximate concentration of the compound giving 50% inhibition of PrPres formation, relative to the vehicle-treated control (IC_{50}), was estimated by signal intensity. To control for the detection limits of western blotting, we performed additional experiments utilizing sodium phosphotungstic acid (PTA) precipitation, which is the most sensitive technique presently available to detect PrPres (Safar *et al.* 1998). The PTA precipitation was undertaken on cell lysates of ScN2a treated with BF-168 at a designated concentration. The resulting pellets were collected by centrifugation and then analyzed by immunoblotting as described above.

In vivo treatment in model animals

BF-168 solution (4 mg/kg body weight) or vehicle alone was injected intravenously to experimental animals ($n = 5$) once a week. The treatment was started at 2 weeks after injection for Tg7 mice and at 4 weeks after injection for Tga20 mice, and repeated for 4 weeks. A continuous subcutaneous infusion of BF-168 was also given to Tga20 mice ($n = 5$) using an Alzet osmotic pump (Durect, Cupertino, CA, USA). In accordance with the manufacturer's instructions, each pump was filled with BF-168 solution at the designated doses and placed in a subcutaneous area of the back at 4 weeks after injection. The animals showed no apparent adverse effects of the treatment and were monitored 5 days a week until obvious clinical signs appeared. Statistical significance was analyzed by one-way ANOVA followed by Scheffé's method for multiple comparisons.

Results

Brain uptake and toxicity

We designed and synthesized novel styrylbenzoxazole derivatives (Table 1), styrylbenzothiazole and styrylbenzoimidazole derivatives (Table 2) with more efficient permeability of the BBB and less toxicity. Values for brain uptake at 2 min after intravenous injection of the compounds were in the 2.4–17.0%ID/g range, indicating a satisfactory level for imaging probes. Their washouts from the brain varied, with the ratio of %ID/g at 2 min to that at 30 min after injection ranging from 1.0 to 56.9. Acute toxicity was tested by administering each compound intravenously at ~10 mg/kg body weight into normal ICR mice. No apparent toxic effect was observed with any of the compounds tested.

PrP imaging ability

Imaging of abnormal PrP deposition by the compounds was first performed in brain sections of human TSE. The compounds fluorescently labeled most of the PrP plaques in cerebellar cortices of both GSS cases (Fig. 1a, representative data). Among sections from the sporadic CJD cases, PrP deposition was labeled only in a case with plaques (Fig. 1c). In the cerebral cortex from the variant CJD case, large core plaques were detectable, whereas the majority of immunopositive aggregates were not labeled (Fig. 1e). In contrast, no fluorescence signal was identified in sections from the dura CJD case or the other sporadic CJD cases that

Table1 Chemical structure, PrPres inhibition and brain uptake of styrylbenzoxazole derivatives including BF-168

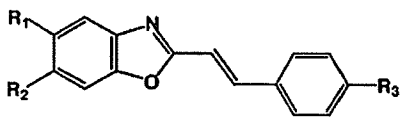

Compound	R_1	R_2	R_3	IC_{50} (nM)[a]	Brain uptake (%ID/g)[b] 2 min	Brain uptake (%ID/g)[b] 30 min	Ratio of 2 to 30 min brain uptake
BF-168	H	$O(CH_2)_2F$	$NH(CH_3)$	0.4	3.9[c]	1.6	2.4
BF-125	H	H	$N(C_2H_5)_2$	10.2	3.0	3.0	1.0
BF-133	F	H	$N(CH_3)_2$	1.6	5.5	3.8	1.4
BF-135	NO_2	H	$N(CH_3)_2$	< 1	NT[d]	NT	-
BF-140	F	H	NH2	< 1	5.5	1.1	5.0
BF-145	F	H	$NH(CH_3)$	< 1	4.4	1.6	2.8
BF-148	H	F	$N(CH_3)_2$	< 1	NT	NT	-
BF-165	H	H	$NH(CH_3)$	7.1	7.2	NT	-
BF-169	H	OH	$NH(CH_3)$	2.4	NT	NT	-
BF-173	I	H	NH_2	2.2	NT	NT	-
BF-180	I	H	$NH(CH_3)$	8.5	2.4	1.8	1.3
BF-191	H	H	Cl	1.8	12.0	1.7	7.1
BF-208	H	H	F	< 1	11.0	0.53	20.8
N-282	H	H	$N(CH_3)_2$	2.1	4.0	1.7	2.4
N-407	H	H	H	< 1	17.0	0.99	17.2

[a]IC_{50}, approximate concentration of a compound giving 50% inhibition of PrPres formation relative to the control in ScN2a cells.
[b]%ID/g, percentage of injected dose per gram in the brains of normal mice.
[c]already reported in the previous work (Okamura *et al.*, 2004).
[d]NT, not tested.

Table 2 Chemical structure, PrPres inhibition and brain uptake of styrylbenzothiazole and styrylbenzoimidazole derivatives

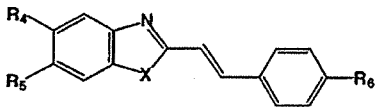

Compound	X	R_4	R_5	R_6	IC_{50} (nM)[a]	Brain uptake (%ID/g)[b] 2 min	Brain uptake (%ID/g)[b] 30 min	Ratio of 2 to 30min brain uptake
BF-124	S	H	H	$N(C_2H_5)_2$	18.1	2.4	2.5	1.0
BF-162	S	F	H	$N(CH_3)_2$	1.4	NT[c]	NT	-
N-276	S	H	H	$N(CH_3)_2$	< 1	NT	NT	-
N-438	S	H	H	H	< 1	11.0	2.0	5.5
BF-126	NH	H	H	$N(C_2H_5)_2$	21	7.2	0.16	45
BF-166	NH	F	H	$N(C_2H_5)_2$	1.1	NT	NT	-
N-457	NH	H	H	Cl	< 1	7.1	0.21	33.8
N-491	NH	H	H	H	1.9	7.4	0.13	56.9

[a]IC_{50}, approximate concentration of a compound giving 50% inhibition of PrPres formation relative to the control in ScN2a cells.
[b]%ID/g, percentage of injected dose per gram in the brains of normal mice.
[c]NT, not tested.

included perivacuolar and/or synaptic PrP deposition (data not shown). Background staining was barely observed after rinsing off the excess compound. Immunohistochemical analysis of PrP revealed that the compounds achieved high-specificity labeling (Figs 1b, d and f). The compounds displayed no signal in control sections without amyloid lesions (data not shown).

Similar results were observed in experimental mice. PrP plaques were specifically labeled in brain sections of Tg7 mice infected with the 263K strain, and there was no PrP immunopositive reaction or fluorescence signal in brain sections of uninfected mice (data not shown). We performed *in vivo* experiments using presymptomatic Tg7 mice at a later stage of TSE. A typical image is shown in Fig. 1(g); peripheral administration of BF-168 fluorescently labeled plaques in the cerebral white matter, indicating that the compound efficiently entered the brain and bound to coarse PrP deposits. Subsequent immunostaining verified the specificity and sensitivity for PrP (Fig. 1h). Non-specific staining, such as cerebrovascular labeling, was occasionally observed at 4 h after injection of 5 mg/kg BF-168, but not after 8 h or more. The stability of the fluorescence signals was examined at various time points up to 24 h after injection and the dye–PrP complex remained visible at the latest time. In contrast, there was no significant labeling after an injection of BF-168 into uninfected animals, or after an injection of vehicle alone to terminally ill Tg7 mice. Similar results were obtained for Tga20 mice infected with the RML strain, although plaques were less frequently detected (data not shown).

Anti-prion activity *in vitro*

The anti-prion activities of the compounds were investigated using ScN2a cells, which are most commonly used for drug screening for TSE treatment. Styrylbenzoxazole derivatives, including BF-168, were evaluated and confirmed to inhibit PrPres formation with IC_{50} values in the nanomolar or subnanomolar range (Fig. 2a and Table 1). Styrylbenzothiazole and styrylbenzoimidazole derivatives were similarly potent, in a dose-dependent manner, within a non-toxic dose range (~10 μM) (Table 2). Treatment with vehicle alone showed no inhibitory effect compared with untreated controls (Fig. 2a). We utilized PTA precipitation, which increases the sensitivity of western blotting, and confirmed the potency of BF-168 at a concentration of 10 times the IC_{50}. Furthermore, radiographic film was exposed to the blotted PVDF membranes for 10 times longer than usual before developing. No significant signals were visualized, whereas bands representing the vehicle-treated control were so strong as to be already saturated (Fig. 2b). To determine whether the efficacy was transient, ScN2a cells treated with 10 nM BF-168 were further cultured for 2 weeks in the absence of BF-168. PrPres signals never reappeared, even through four passages after discontinuation of the treatment (Fig. 2c). To exclude the possibility of interference with immunodetection, BF-168 solution at a final concentration of 10 nM was added to a lysate of untreated ScN2a cells before proteinase K digestion. PrP signals were not affected (data not shown). Nor was any alteration observed in cellular PrP level of N2a cells after treatment with 10 nM BF-168 (Fig. 2d).

To investigate whether the efficacy of the compounds depends on pathogen strain, we tested BF-168 in three N2a58 cell lines individually infected with different strains. As shown in Table 3, BF-168 was only effective in N2a58 cells infected with the RML strain, although the inhibitory activity was not as strong as in ScN2a cells (~1 μM). In contrast, BF-168 was ineffective in the same N2a58 cells infected with the 22L or Fukuoka-1 strains up to 10 μM, a dose at which the compound showed host cytotoxicity.

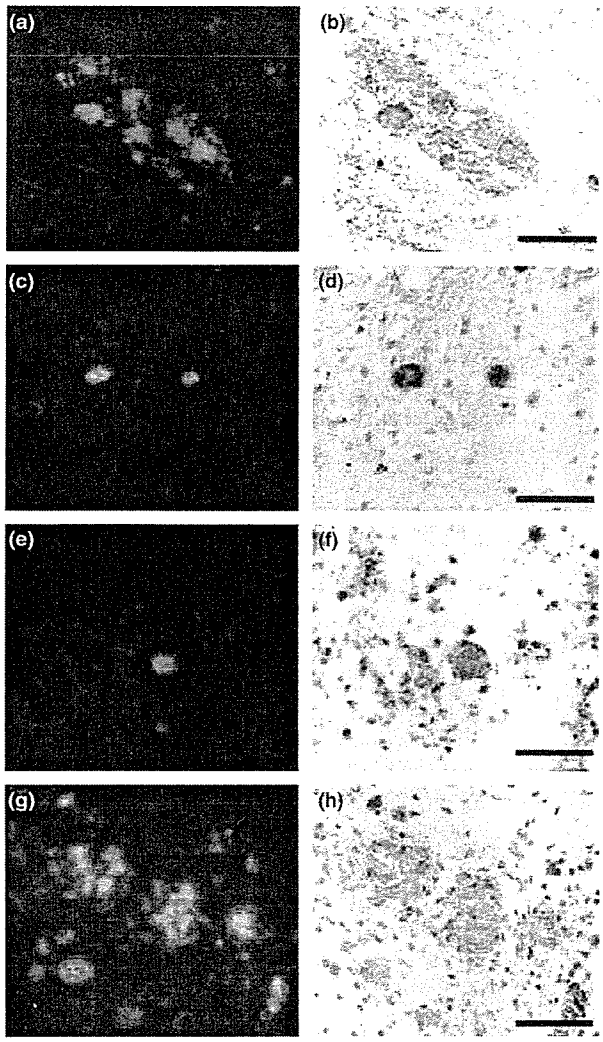

Fig. 1 PrP imaging *in vitro* and *in vivo*. BF-168 fluorescently labeled PrP deposition in a cerebellar section from the case of GSS (a), and in cerebral sections from cases of sporadic CJD with plaques (c) and variant CJD (e). Similar results were obtained from the brains of living TSE-infected mice that were intravenously injected with BF-168 solution (0.5 mg/kg). BF-168 detected PrP deposition in the cerebral white matter between the cortex and hippocampus (g). Sections (a, c, e and g) were subsequently immunoassayed for PrP (b, d, f and h). Bars represent 100 μm (a–f) and 25 μm (g and h).

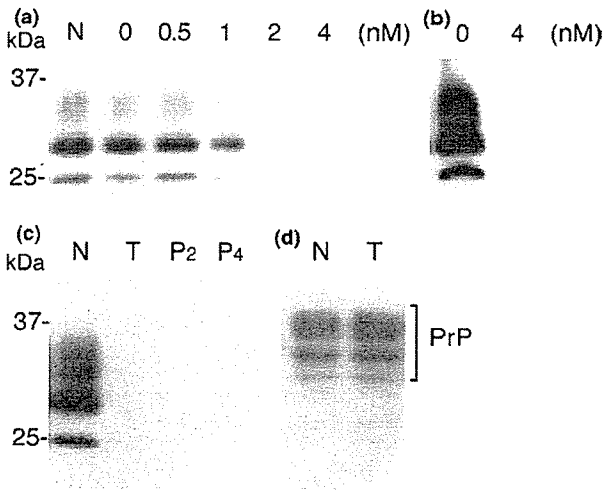

Fig. 2 Effects of BF-168 on PrP expression in ScN2a and N2a cells. BF-168 was added at the designated concentrations to freshly passaged cells. PrPres formation in ScN2a cells was inhibited in a dose-dependent manner (a). To exclude the sensitivity limit of immunoblotting, ScN2a cells treated with 4 nM BF-168 were also analyzed by sodium PTA, and no significant signals were visualized (b). ScN2a cells treated with 10 nM BF-168 were maintained for an additional four passages, and the PrPres signal was not restored in the absence of BF-168 (c). PrP expression was not affected in N2a cells that were grown in the presence of 10 nM BF-168 (d). Lane N, untreated cells; lane 0, cells treated with vehicle alone; lane T, cells treated with 10 nM BF-168; lanes P_2 and P_4, cells following two and four passages after treatment respectively. Bars on the left indicate molecular size markers at 37 and 25 kDa.

Table 3 Anti-prion activities (IC_{50}) of BF-168 in various types of TSE-infected cells

Host cells	Pathogen strains		
	RML	22L	Fukuoka-1
N2a	0.4 nM	None[a]	–[b]
N2a58	~1 μM	None	None
L929	~10 nM	–	–
GT1-7	–	None	–

[a]None, no significant PrPres inhibition up to 10 μM, a dose that affect the rate of cell growth.
[b], not available.

Furthermore, we established L929 cells stably infected with the RML strain. BF-168 inhibited PrPres formation in the RML-infected L929 cells with an IC_{50} in the nanomolar range. We also tested potency against the 22L strain in two other cell lines, N2a and GT1-7 cells. BF-168 was ineffective in either cell line infected with the 22L strain. Other compounds tested here demonstrated similar results (data not shown). These results suggest that the styrylbenzoxazole derivatives exert their inhibitory activity on PrPres formation in a strain-dependent, but not a host cell-dependent, manner.

Therapeutic efficacy *in vivo*

The therapeutic activity of the compounds *in vivo* was assayed in two different mouse models using BF-168 as a representative. Treatment was initiated 2–4 weeks after TSE infection and repeated once a week for 4 weeks. The dosage at a single administration corresponded to a dose sufficient to detect PrP plaques. As shown in Table 4, there was no

Table 4 Effects of BF-168 treatment on intracerebrally TSE-infected mice

Mouse - pathogen strain	*n*	Dose (mg/kg/week)	Administration	Incubation period Mean ± SD (days)
Tg7 - 263K				
	7	Control	-	49.4 ± 1.9
	5	Vehicle	i.v.[a]	50.2 ± 4.1
	5	4	i.v.	52.2 ± 2.6
Tga20 - RML				
	7	Control	-	66.6 ± 1.6
	5	Vehicle	i.v.	64.8 ± 1.6
	5	4	i.v.	72.2 ± 2.5*
	5	10	s.c.[b]	66.0 ± 3.1

* $p < 0.001$ versus the oher groups.
[a]i.V., intravenous injection of BF-168 once a week for 4 weeks from 2 weeks p.i. for Tg7, or 4 weeks p.i. for Tga20.
[b]s.c., continous subcutaneous infusion of BF-168 for 4 weeks from 4 weeks p.i.

significant difference in incubation periods between groups of Tg7 mice infected intracerebrally with the 263K strain, with or without treatment. In contrast, intravenous injection with 4 mg/kg BF-168 significantly prolonged the incubation period (~ 11.4%) of Tga20 mice intracerebrally infected with the RML strain.

In another trial, we used osmotic pumps filled with BF-168 solution, assuming that the route of administration is a key issue. The pump worked continuously for 4 weeks, and the total dosage for the duration was selected to correspond to two to three times that administered intravenously. Subcutaneous infusion of BF-168, however, did not prolong incubation periods of Tga20 mice intracerebrally infected with the RML strain (Table 4). There was no significant difference in incubation period in either group of infected mice between untreated controls and controls treated with vehicle alone.

Discussion

Our results show that styrylbenzoazole derivatives represent candidates for imaging probes as well as therapeutic drugs for TSE. It has been increasingly necessary to develop minimally non-invasive methods for recognizing early clinical infection and evaluating treatment of TSE. We have already focused on two β-amyloid imaging probes and reported them as potential agents for TSE (Ishikawa *et al.* 2004). The problem is, however, that they seemed to have practical limitations because of inadequate brain uptake and washout. Here, we confirmed that novel styrylbenzoazole derivatives clearly labeled PrP plaques *in vitro* and BF-168, the parent compound, entered the brain and labeled PrP plaques *in vivo*, even at a 20-fold lower dose than the probes we previously reported. In brain uptake studies, all of the compounds showed BBB permeability with >1%ID/g, which is proposed to be sufficient for neuroimaging probes. The background staining of 0.5 mg/kg BF-168 was almost absent at 4 h after administration, suggesting excellent clearance from the brain.

Most of styrylbenzoazole derivatives labeled β-amyloid aggregates in AD specimens in this study (data not shown) as well as in the previous study on Alzheimer's (Okamura *et al.* 2004). This is also observed with 2-(1-[6-[(2-fluoroethyl)(methyl)amino]-2-naphthyl]ethylidene)malononitrile (FDDNP), one of the promising agents for imaging β-amyloid deposition. FDDNP has been reported to label PrP plaques in brain sections, and is a candidate for imaging PrP deposition (Bresjanac *et al.* 2003). These findings imply lack of disease specificity, but the compounds should still be useful for some types of TSE, because anatomical distributions of amyloid deposition are characteristically different between diseases. Pathological changes including amyloid deposition of AD brain are always observed in the hippocampus but not in the cerebellum, whereas those of TSE tend to be absent from the hippocampus but to be demonstrated in the cerebellum.

Styrylbenzoazole derivatives detected predominantly PrP plaques, especially in specimens of sporadic CJD with plaques and variant CJD. However, their ability to detect synaptic or perivacuolar PrP deposition remains inconclusive, until more sensitive investigations, such as autoradiography, are available. The compounds tested in this study can be used with radionuclides. ^{18}F-radiolabeled BF-168, which has already been employed for labeling of β-amyloid deposits including both neuritic and diffuse plaques in AD brain (Okamura *et al.* 2004), may be a suitable tool for investigating whether PrP deposition, other than plaque type, can be detected.

This study demonstrated that styrylbenzoazole derivatives have more potent anti-prion activity than the amyloid imaging probes reported previously (Ishikawa *et al.* 2004). Although the neuropathological processes remain unclear, one of the most likely strategies for TSE treatment is a small-molecule drug that can enter the brain and inhibit abnormal PrP formation. It is important to emphasize that styrylbenzoazole derivatives have a wide concentration safety margin, and some were effective even at subnanomolar doses in ScN2a cells. Dozens of drug candidates for TSE have been reported to date but, as far as we know, the most potent inhibitor class for abnormal PrP formation in ScN2a cells is specific blocking antibodies with an IC_{50} in the nanomolar range (Peretz *et al.* 2001).

BF-168 showed no apparent alteration in cellular PrP expression level in N2a cells, and also labeled abnormal PrP deposition both *in vitro* and *in vivo*. These data suggest that styrylbenzoazole derivatives might interact directly with abnormal PrP molecules to block the conversion of normal to abnormal PrP. The structure–activity relationship, examined by introducing side-chain or functional groups into the benzoazole and/or benzene rings, demonstrates that the inhibitory potency is not always the same, even among

closely related compounds (data not shown). Although we could not obtain any insight into inhibitory mechanisms, the efficacy of BF-168 was dependent on pathogen strain, and this is consistent with our previous work using three types of cell lines (Ishikawa *et al.* 2004). In an attempt to further explore strain dependency, we tested three different pathogen strains in one host cell line, and three different host cell lines with one pathogen strain. BF-168 inhibited abnormal PrP formation in all three types of RML-infected cells, including ScN2a cells. By contrast, BF-168 did not demonstrate any inhibitory activity in the 22L- or Fukuoka-1-infected cells. It is well known that prion strains differ in their biological profiles such as the degree of glycosylation and the conformation of PrP molecules. In the imaging experiments we confirmed that the compound bound to a certain type of abnormal PrP aggregates. Thus, it was assumed that the therapeutic efficacy might be based on blocking certain interactions between normal and abnormal PrP, and that BF-168 might recognize the PrP conformation. However, considering a discrepancy in the *in vivo* experiment between PrP imaging and treatment using infected Tg7 mice, these inferences remain unsupported and the precise mechanism of the strain-dependent efficacies needs to be elucidated.

Kocisko *et al.* (2004) reported that anti-prion activity *in vitro* does not always correlate with that *in vivo*. With *in vivo* testing, there are many variables, such as inoculation route, dosing protocol and pathogen strain. The efficacy differed according to the BF-168 administration route in Tga20 mice, even though the dose administered subcutaneously for the same duration was no less than that administered intravenously. This might be due to differences in stability and clearance of BF-168 in relation to the route of administration.

Most previous therapeutic investigations showed a significant benefit *in vivo* when the treatment was started before, or soon after, peripheral TSE infection. Although the efficacy of BF-168 was limited, it is noteworthy that we obtained significant results with peripheral administration at a later stage of the intracerebral infection. In addition, BF-168 showed excellent brain uptake and binding affinity towards PrP aggregates *in vivo*, even at a low dose, suggesting that the compound should be a good imaging probe for clinical use. In the treatment of infected Tga20 mice, BF-168 showed almost the same prolongation of the incubation period but with a 10-fold smaller dose than (trans, trans)-1-bromo-2,5-bis-(3-hydroxycarbonyl-4-hydroxy)styrylbenzene (BSB), which we reported previously as one of the amyloid imaging probes applicable for TSE (Ishikawa *et al.* 2004). BF-168 showed a low IC_{50} of 0.4 nM in treatment of ScN2a cells, whereas the IC_{50} of BSB was more than 1000-fold higher (1.4 μM). We decided the dosing protocol for our experimental animals from *in vitro* data, including the ratio of these IC_{50} values, and from an *invivo* imaging experiment in which 0.1 mg BF-168 per injection was enough to detect PrP deposition. It is also necessary to consider washout of the compound from the brain. Further studies are required to examine issues such as dose–response relationships, administration time and dosing conditions. Furthermore, there was a problem in that administration frequency was limited because animal tail tissue was damaged by repetitive intravenous injections. In addition, it should be investigated whether compounds with slower washout from the brain are more suitable as therapeutic agents.

In conclusion, styrylbenzoazole derivatives efficiently entered the brain and labeled pathological PrP deposition, and demonstrated some anti-prion activities both *in vitro* and *in vivo*. Although their efficacy depended on the pathogen strain, these are a new class of compounds with potential as therapeutic drugs and imaging probes for TSE.

Acknowledgements

This study was supported by grants to KD from the Ministry of Health, Labour and Welfare (H16-kokoro-024) and the Ministry of Education, Culture, Sports, Science and Technology 13557118, 14021085, Japan. The authors thank Dr James W. Ironside of the CJD Surveillance Unit, Edinburgh, UK, for providing the variant CJD specimens.

References

Bresjanac M., Smid L. M., Vovko T. D., Petric A., Barrio J. R. and Popovic M. (2003) Molecular-imaging probe 2-(1-[6-[(2-fluoroethyl)(methyl) amino]-2-naphthyl]ethylidene) malononitrile labels prion plaques *in vitro*. *J. Neurosci.* **23**, 8029–8033.

Brown P., Preece M., Brandel J. P. *et al.* (2000) Iatrogenic Creutzfeldt–Jakob disease at the millennium. *Neurology* **55**, 1075–1081.

Caughey B. and Raymond G. J. (1993) Sulfated polyanion inhibition of scrapie-associated PrP accumulation in cultured cells. *J. Virol.* **67**, 643–650.

Doh-ura K., Mekada E., Ogomori K. and Iwaki T. (2000) Enhanced CD9 expression in the mouse and human brains infected with transmissible spongiform encephalopathies. *J. Neuropathol. Exp. Neurol.* **59**, 774–785.

Fischer M., Rulicke T., Raeber A., Sailer A., Moser M., Oesch B., Brandner S., Aguzzi A. and Weissmann C. (1996) Prion protein (PrP) with amino-proximal deletions restoring susceptibility of PrP knockout mice to scrapie. *EMBO J.* **15**, 1255–1264.

Ishikawa K., Doh-ura K., Kudo Y., Nishida N., Murakami-Kubo I., Ando Y., Sawada T. and Iwaki T. (2004) Amyloid imaging probes are useful for detection of prion plaques and treatment of transmissible spongiform encephalopathies. *J. Gen. Virol.* **85**, 1785–1790.

Kocisko D. A., Morrey J. D., Race R. E., Chen J. and Caughey B. (2004) Evaluation of new cell culture inhibitors of protease-resistant prion protein against scrapie infection in mice. *J. Gen. Virol.* **85**, 2479–2483.

Milhavet O., McMahon H. E., Rachidi W. *et al.* (2000) Prion infection impairs the cellular response to oxidative stress. *Proc. Natl Acad. Sci. USA* **97**, 13 937–13 942.

Nishida N., Harris D. A., Vilette D., Laude H., Frobert Y., Grassi J., Casanova D., Milhavet O. and Lehmann S. (2000) Successful transmission of three mouse-adapted scrapie strains to murine neuroblastoma cell lines overexpressing wild-type mouse prion protein. *J. Virol.* **74**, 320–325.

Okamura N., Suemoto T., Shimadzu H. *et al.* (2004) Styrylbenzoxazole derivatives for *in vivo* imaging of amyloid plaques in the brain. *J. Neurosci.* **24**, 2535–2541.

Okamura N., Suemoto T., Furumoto S. *et al.* (2005) Quinoline and benzimidazole derivatives: candidate probes for *in vivo* imaging of tau pathology in Alzheimer's disease. *J. Neurosci.* **25**, 10 857–10 862.

Peretz D., Williamson R. A., Kaneko K. *et al.* (2001) Antibodies inhibit prion propagation and clear cell cultures of prion infectivity. *Nature* **412**, 739–743.

Prusiner S. B. (1991) Molecular biology of prion diseases. *Science* **252**, 1515–1522.

Race R. E., Caughey B., Graham K., Ernst D. and Chesebro B. (1988) Analyses of frequency of infection, specific infectivity, and prion protein biosynthesis in scrapie-infected neuroblastoma cell clones. *J. Virol.* **62**, 2845–2849.

Race R. E., Priola S. A., Bessen R. A., Ernst D., Dockter J., Rall G. F., Mucke L., Chesebro B. and Oldstone M. B. (1995) Neuron-specific expression of a hamster prion protein minigene in transgenic mice induces susceptibility to hamster scrapie agent. *Neuron* **15**, 1183–1191.

Safar J., Wille H., Itri V., Groth D., Serban H., Torchia M., Cohen F. E. and Prusiner S. B. (1998) Eight prion strains have PrP(Sc) molecules with different conformations. *Nat. Med.* **4**, 1157–1165.

Vorberg I., Raines A., Story B. and Priola S. A. (2004) Susceptibility of common fibroblast cell lines to transmissible spongiform encephalopathy agents. *J. Infect. Dis.* **189**, 431–439.

Will R. G., Ironside J. W., Zeidler M. *et al.* (1996) A new variant of Creutzfeldt–Jakob disease in the UK. *Lancet* **347**, 921–925.

Journal of Pathology
J Pathol 2006; **209**: 484–491
Published online 9 June 2006 in Wiley InterScience
(www.interscience.wiley.com) **DOI:** 10.1002/path.2009

Original Paper

Clusterin expression in follicular dendritic cells associated with prion protein accumulation

K Sasaki,[1]* K Doh-ura,[2] JW Ironside,[3] N Mabbott[4] and T Iwaki[1]

[1] *Department of Neuropathology, Neurological Institute, Graduate School of Medical Sciences, Kyushu University, Fukuoka 812-8582, Japan*
[2] *Division of Prion Biology, Department of Prion Research, CTAAR, Tohoku University School of Medicine, Sendai 980-8575, Japan*
[3] *National CJD Surveillance Unit, University of Edinburgh, Western General Hospital, Edinburgh EH4 2XU, UK*
[4] *Institute for Animal Health, Edinburgh EH9 3JF, UK*

*Correspondence to:
Dr K Sasaki, Department of Neuropathology, Neurological Institute, Graduate School of Medical Sciences, Kyushu University, Fukuoka 812-8582, Japan.
E-mail:
ksasaki@np.med.kyushu-u.ac.jp

Received: 26 January 2006
Revised: 18 March 2006
Accepted: 28 March 2006

Abstract

Peripheral accumulation of abnormal prion protein (PrP) in variant Creutzfeldt–Jakob disease and some animal models of transmissible spongiform encephalopathies (TSEs) may occur in the lymphoreticular system. Within the lymphoid tissues, abnormal PrP accumulation occurs on follicular dendritic cells (FDCs). Clusterin (apolipoprotein J) has been recognized as one of the molecules associated with PrP in TSEs, and clusterin expression is increased in the central nervous system where abnormal PrP deposition has occurred. We therefore examined peripheral clusterin expression in the context of PrP accumulation on FDCs in a range of human and experimental TSEs. PrP was detected immunohistochemically on tissue sections using a novel highly sensitive method involving detergent autoclaving pretreatment. A dendritic network pattern of clusterin immunoreactivity in lymphoid follicles was observed in association with the abnormal PrP on FDCs. The increased clusterin immunoreactivity appeared to correlate with the extent of PrP deposition, irrespective of the pathogen strains, host mouse strains or various immune modifications. The observed co-localization and correlative expression of these proteins suggested that clusterin might be directly associated with abnormal PrP. Indeed, clusterin immunoreactivity in association with PrP was retained after FDC depletion. Together these data suggest that clusterin may act as a chaperone-like molecule for PrP and play an important role in TSE pathogenesis.

Keywords: prion; clusterin; follicular dendritic cell; immunohistochemistry; detergent autoclaving pretreatment; immune deficiency

Introduction

Transmissible spongiform encephalopathy (TSE) is the generic term for the fatal neurodegenerative diseases associated with abnormal prion protein (PrP) deposition in the central nervous system (CNS). Human TSE diseases include Creutzfeldt–Jakob disease (CJD), Gerstmann–Sträussler–Scheinker disease, fatal familial insomnia, and kuru. In cases of variant CJD, transmission is thought to have occurred from exposure to bovine spongiform encephalopathy (BSE)-contaminated meat via the oral route [1–3]. In cases of variant CJD and some animal TSE models, peripheral accumulation of abnormal PrP occurs in the lymphoreticular system, within the lymphoid follicles of spleens, lymph nodes, Peyer's patches, and tonsils [4–6]. In these regions, abnormal PrP accumulates on the surfaces of follicular dendritic cells (FDCs) from an early stage of the disease [7], followed by CNS involvement via the peripheral nervous system [8,9].

Clusterin (apolipoprotein J) is a heterodimeric glycoprotein and is expressed in a variety of mammalian tissues. It is considered to have a variety of functions, including inhibition of complement-mediated cytolysis by binding to the membrane attack complex [10]; regulation of apoptosis [11]; and as a survival factor for germinal centre B cells [12]. We have reported that, during TSE disease, clusterin is associated with deposits of abnormal PrP in the CNS [13]. In the CNS of TSE-affected subjects, clusterin co-localizes with the extracellular plaque-type PrP deposits. Clusterin expression is also up-regulated within lesions of synaptic PrP deposition, even though no co-localization is observed. As clusterin interacts with a range of other molecules [14,15], these findings suggest that secreted clusterin might act as a chaperone-like molecule for PrP. Previous *in vitro* investigations have shown that clusterin is induced in astrocytes by PrP fragments reminiscent of the abnormal PrP isoform [16], and prevents their fibrillar aggregation [17].

FDCs also express clusterin [12]. Therefore we investigated whether clusterin expression in the lymphoreticular system is likewise affected by TSE infection, and associated with the extracellular accumulation of abnormal PrP on FDCs.

Materials and methods

Antibodies

The antibodies used included anti-human PrP C-terminal (rabbit polyclonal, IBL, Japan; raised against a peptide mapping to the C-terminus of human PrP, cross-reacts with mouse PrP), anti-human PrP N-terminal (rabbit, IBL; raised against a peptide mapping to the N-terminus of human PrP, cross-reacts with mouse PrP), anti-human PrP (mouse monoclonal, 3F4, Signet, MA, USA; recognizing amino acid residues 109–112, cross-reacts with hamster PrP), anti-mouse clusterin (goat polyclonal, M-18, Santa Cruz, CA, USA; raised against a peptide mapping to the C-terminus of mouse clusterin), anti-human clusterin (goat, C-18, Santa Cruz; raised against a peptide mapping to the C-terminus of human clusterin), or anti-human clusterin (goat, Chemicon, CA, USA; raised against a purified clusterin from human plasma), anti-mouse CD21/CD35 (CR2/CR1, rat monoclonal, 7G6, PharMingen, CA, USA), anti-human CD35 (CR1, mouse, Ber-MAC-DRC, Dako, Denmark). We assessed two anti-human clusterin antibodies by immunohistochemistry and verified that both gave similar results [13].

Mouse models

Non-transgenic NZW mice and transgenic Tga20 mice [18,19] that express high amounts of mouse PrP were inoculated intraperitoneally (i.p.) with the Fukuoka-1 mouse-passaged scrapie agent strain (NZW/Fu-1, Tga20/Fu-1, respectively). Transgenic Tg7 mice [8,20] that express high amounts of hamster PrP on a mouse-PrP knockout background were inoculated i.p. with the 263K hamster-passaged scrapie agent strain (Tg7/263K). Permission for these animal experiments was obtained from the Animal Experiment Committee of Kyushu University.

Where indicated, C57BL/Dk mice were inoculated either orally or i.p. with the ME7 mouse-passaged scrapie agent strain (C57BL/ME7 mice). To deplete FDCs temporarily, C57BL/Dk mice were given a single i.p. injection of a fusion protein containing the soluble lymphotoxin β receptor domain linked to the Fc portion of human IgG1 (LTβR-Ig) or 100 μg polyclonal human IgG (hu-Ig) (Sandoglobulin®) as a control [21,22]. Where indicated, treatment was given 3 days before (−3 dpi) oral inoculation, or 14 or 42 days after (14 dpi & 42 dpi, respectively) i.p. inoculation with the ME7 scrapie agent strain as described [21,22]. Spleens were analysed 3 days after treatment; Peyer's patches were analysed 70 days after inoculation with the scrapie agent. Mice deficient in interleukin- (IL-) 6 (IL-6-knockout (KO) mice, on a 129/Sv × C57BL/6 background) possess FDC networks but have impaired germinal centres [23]. IL-6-KO mice, and 129/Sv × C57BL/6 immunocompetent wild-type mice, were also inoculated i.p. with the ME7 mouse-passaged scrapie agent strain. Permission for these animal experiments was obtained from the Ethical Review Committee at the Institute for Animal Health, Edinburgh, UK.

Table 1 summarizes the profiles of the mouse lines used in this study.

Human CJD cases

Paraffin-embedded sections of spleens, lymph nodes, appendices, and tonsils were examined from five cases of variant CJD (three males, two females, age range 17–39 years, duration of clinical illness 7–33 months) from the UK National CJD Surveillance Unit, University of Edinburgh, UK. Spleen sections were also examined from four cases of sporadic CJD (two males, two females, age range 55–69 years, duration of clinical illness 4–30 months) from the Department of Neuropathology, Kyushu University. The diagnosis of variant or sporadic CJD was confirmed by postmortem examination. Each case had consent for use of autopsy tissues for research purposes and local Ethics Committee approval for the use of human autopsy tissues from patients with CJD for research was also obtained.

Table 1. Profiles of mouse lines

Line	Background	Modification of PrP expression	PrP^c on FDCs	Reference	Inoculum	PrP^{sc} on FDCs
NZW wild		None	+		Fukuoka-1	+
C57BL/Dk Wild		None	+		ME7	+
Tg7	C57BL/10	MoPrP knockout Overexpress HaPrP under control of the endogenous MoPrP promoter	+	8,20	263K	−
Tga20	129/Sv × C57BL/6	MoPrP knockout Overexpress MoPrP under control of the endogenous MoPrP promoter	−*	18,19	Fukuoka-1	−
IL-6 KO	129/Sv × C57BL/6	None	+	23	ME7	+

MoPrP = mouse PrP; HaPrP = hamster PrP; PrP^c = cellular PrP expression on the FDCs; PrP^{sc} = abnormal PrP accumulation on FDCs of scrapie affected mice; (−) negative; (+) positive.

* Negative on FDCs but some cells within the paracortical T-cell area express PrP^c [19].

The inocula indicated were applied to the respective mouse lines in this study.

Immunohistochemistry

To enhance the detection of PrP by immunohistochemistry (IHC), formalin-fixed, paraffin-embedded sections were pretreated by hydrolytic autoclaving (1–2 mM HCl, 121 °C, 10 min) or a protocol using formic acid, guanidine thiocyanate, and hydrated autoclaving as previously reported [24,25]. We also performed an autoclaving pretreatment with Target Retrieval Solution (Dako) or buffer solution with detergent. A variety of detergents were examined including, Triton X-100 and Tween-20 as non-ionic detergents and sodium dodecyl sulphate as an ionic detergent. We found that non-ionic detergents enhanced PrP detection to a similar degree, whereas the ionic detergent enhanced PrP detection sensitivity, but caused considerable tissue damage. Autoclaving the sections in 0.1% Triton X-100 in 50 mM Tris-HCl, pH 7.6, 121 °C, 20 min, was found to be the most suitable method for the detection of abnormal PrP accumulation on FDCs, and was used in this study (hereinafter referred to as the detergent autoclaving method). Increased concentrations of Triton X-100 up to 0.5% did not significantly increase the signal intensity of the PrP detected or affect the degree of tissue damage. This indicated that the detergent autoclaving method had a wider range of optimum detergent concentrations than the HCl in the hydrolytic autoclaving method. Immunoreactions were visualized using diaminobenzidine as a chromogen.

To examine the co-localization of two different proteins on the same section, the first immunoreaction was visualized using 3-amino-9-ethylcarbazole (AEC; Vector, CA, USA), mapped, and photographed. The section was then decolourized by immersing it in ethanol, and the second immunohistochemical procedure was performed with the other primary antibody. Double immunofluorescence was also performed to reveal sites of co-localization.

Results

Experiments demonstrated that the detergent autoclaving method was the most useful for detecting PrP by IHC. This was particularly evident on sections of spleen tissue, where this method drastically improved the signal intensity for PrP accumulated on FDCs in comparison with sections treated by the HCl autoclave method (Figure 1A and B, respectively). Table 2 shows comparisons between this detergent autoclaving method and conventional techniques for IHC detection of PrP. On human brain samples, most of the different types of PrP deposition could be detected by the detergent autoclaving method as well as by conventional techniques (Figure 1C and 1D, respectively). However, the detergent autoclaving method

Table 2. Comparison of the methods of immunohistochemistry for PrP

	Detergent autoclaving	HCl autoclaving [24]	Three steps [25]
PrP signal intensity			
Synaptic	+ ~ ++	++	+ ~ ++
Plaque	++	++	++
FDCs (mouse)	++	+	++
Background	Low	High	Moderate
Tissue damage	Low	High	Moderate
Simplicity	Simple	Moderate	Complicated

(+) positive; (++) strongly positive.
In the three steps method samples are pretreated with formic acid, guanidine thiocyanate, and hydrated autoclaving.

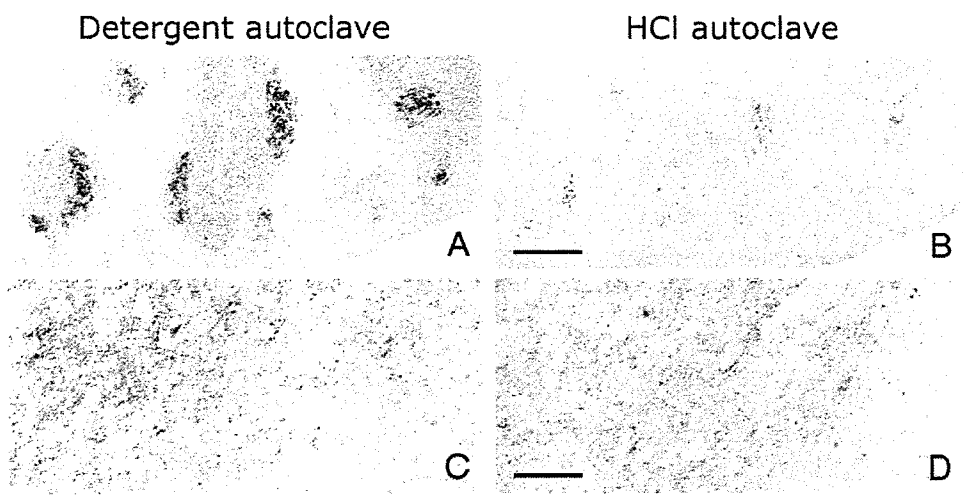

Figure 1. Effect of detergent autoclaving pretreatment on the detection of PrP by immunohistochemistry. (A, B) Serial sections of spleen from TSE-infected mice (NZW mouse inoculated with Fukuoka-1 strain) were immunostained for PrP. The detergent autoclaving method (A) dramatically increased the signal intensity of the PrP immunoreaction and lowered non-specific background staining in comparison with the HCl autoclaving method (B). (C, D) Serial sections of cerebral cortex from a case with sporadic CJD immunostained for PrP. Immunoreactivity for PrP is rather weak on sections pretreated by the detergent autoclaving method (C) in comparison with those pretreated by the HCl autoclaving method (D). However, abnormal fine granular deposits of PrP are detected by both methods. Bars: 200 μm (A, B), 100 μm (C, D)

decreased background staining,' which facilitated the double immunofluorescence technique in this study.

We examined the lymphoreticular system of mouse models of TSE. In the spleens of scrapie agent-inoculated NZW/Fu-1 ($n = 5$) and C57BL/ME7 mice ($n = 3$), abnormal PrP accumulated on the dendritic network of FDCs as the disease progressed (Figure 2E), but not in the spleens of uninoculated NZW mice ($n = 5$) (Figure 2B) or scrapie agent-inoculated Tg7/263K ($n = 5$) or Tga20/Fu-1 mice ($n = 3$)(data not shown). The apparent lack of cellular PrP expression by FDCs in the spleens of Tga20 mice probably prevents abnormal PrP amplification on these cells [19]. Likewise, after high-dose scrapie inoculation into these transgenic mice, neuroinvasion probably occurs via a putative 'direct neuroinvasion' pathway without the need for prior amplification of abnormal PrP on FDCs [8]. In uninoculated NZW mice, clusterin was constitutively and diffusely expressed in the reticular cells in lymphoid follicles (Figure 2A), as previously reported [26]. However, in the spleens of NZW/Fu-1 mice immunoreactivity for clusterin was

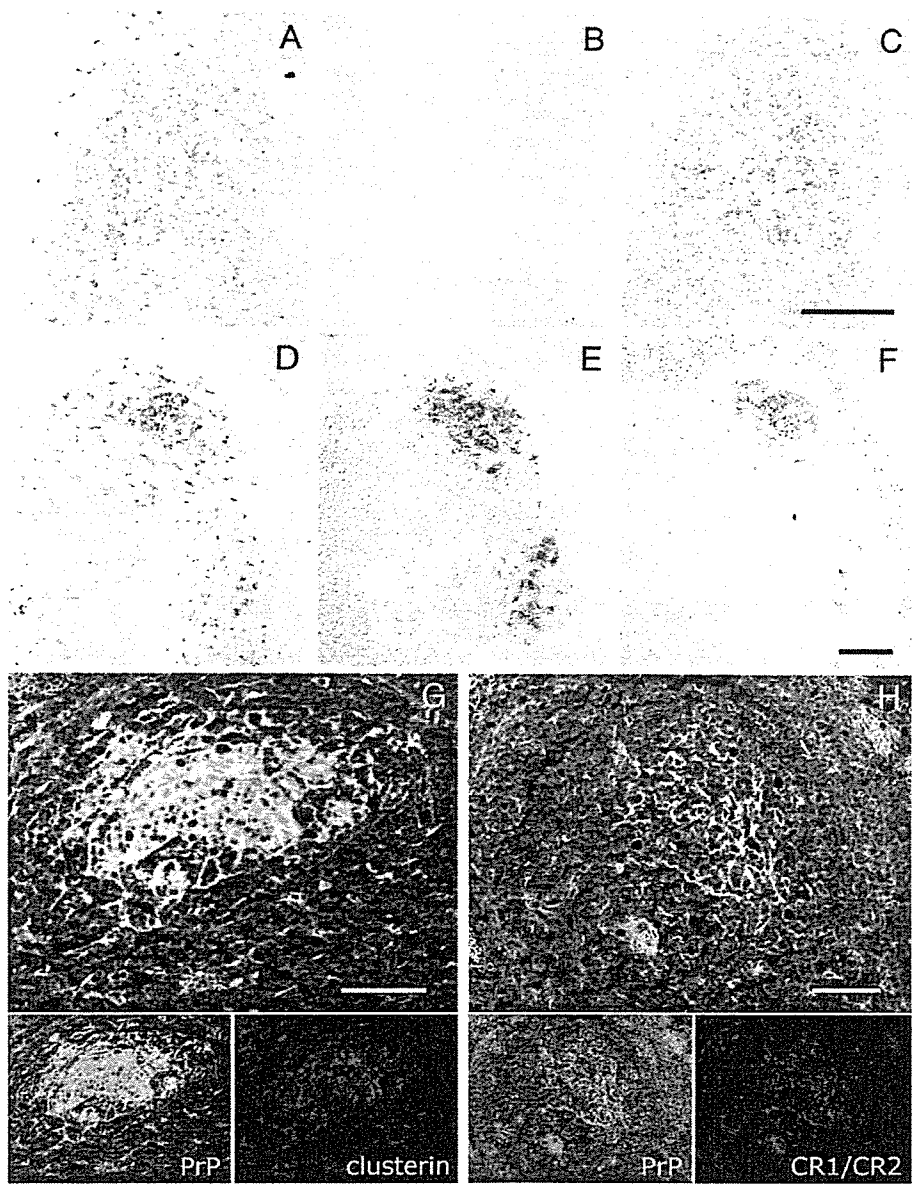

Figure 2. Immunohistochemistry for clusterin expression on FDCs in the spleens of uninoculated and scrapie-inoculated mice. (A–C) Serial sections of uninoculated NZW mouse spleen were immunostained for clusterin (A), PrP (B), and CR1/CR2 (C). Clusterin is constitutively expressed in the reticular cells in the lymphoid follicles of uninoculated mice (A) and not obviously condensed on the dendritic network of FDCs (C). However, increased clusterin expression was observed on FDCs from scrapie-inoculated mice. (D–F) The same section of spleen from the NZW/Fu-1 TSE mouse model was serially immunostained for clusterin (D), PrP (E), and CR1/CR2 (F). Immunoreactivity for clusterin is markedly condensed and increased on the FDCs associated with abnormal PrP accumulation. Similar results were observed in the C57BL/ME7 mouse model. The co-localization of these proteins was also confirmed by double immunofluorescence (G, H). (G) Clusterin (red) and PrP (green). (H) CR1/CR2 (red) and PrP (green). Bars: 100 μm (A–F), 50 μm (G, H)